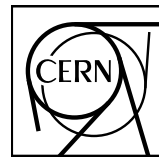


EUROPEAN ORGANIZATION FOR NUCLEAR RESEARCH



CERN-EP-2023-190
29 August 2023

Prompt and non-prompt J/ψ production at midrapidity in Pb–Pb collisions at $\sqrt{s_{\text{NN}}} = 5.02 \text{ TeV}$

ALICE Collaboration*

Abstract

The transverse momentum (p_{T}) and centrality dependence of the nuclear modification factor R_{AA} of prompt and non-prompt J/ψ , the latter originating from the weak decays of beauty hadrons, have been measured by the ALICE collaboration in Pb–Pb collisions at $\sqrt{s_{\text{NN}}} = 5.02 \text{ TeV}$. The measurements are carried out through the e^+e^- decay channel at midrapidity ($|y| < 0.9$) in the transverse momentum region $1.5 < p_{\text{T}} < 10 \text{ GeV}/c$. Both prompt and non-prompt J/ψ measurements indicate a significant suppression for $p_{\text{T}} > 5 \text{ GeV}/c$, which becomes stronger with increasing collision centrality. The results are consistent with similar LHC measurements in the overlapping p_{T} intervals, and cover the kinematic region down to $p_{\text{T}} = 1.5 \text{ GeV}/c$ at midrapidity, not accessible by other LHC experiments. The suppression of prompt J/ψ in central and semicentral collisions exhibits a decreasing trend towards lower transverse momentum, described within uncertainties by models implementing J/ψ production from recombination of c and \bar{c} quarks produced independently in different partonic scatterings. At high transverse momentum, transport models including quarkonium dissociation are able to describe the suppression for prompt J/ψ . For non-prompt J/ψ , the suppression predicted by models including both collisional and radiative processes for the computation of the beauty-quark energy loss inside the quark–gluon plasma is consistent with measurements within uncertainties.

© 2023 CERN for the benefit of the ALICE Collaboration.

Reproduction of this article or parts of it is allowed as specified in the CC-BY-4.0 license.

*See Appendix A for the list of collaboration members

1 Introduction

Quantum chromodynamics (QCD) calculations on the lattice [1–4] predict the existence of the quark–gluon plasma (QGP), a state of strongly-interacting matter characterised by quark and gluon degrees of freedom, expected to be produced at extremely high temperatures and energy densities. Such conditions can be realised in the laboratory by colliding heavy ions at ultra-relativistic energies, enabling the study of the properties of this state of matter, as shown by multiple measurements carried out at the SPS [5, 6], RHIC [7–10] and LHC [11]. Heavy quarks, i.e. charm and beauty, are mainly produced in hard parton–parton scatterings and on a shorter time scale than the QGP formation time at LHC energies ($\tau_{\text{QGP}} \approx 1.5\text{fm}/c$) [12, 13], thus experiencing the full QGP evolution. Charmonia, bound states of a charm and an anti-charm quark, are interesting probes of the QGP. In fact, it was predicted that their production would be suppressed in this medium due to static colour screening resulting from the high density of colour charges inside it [14] or due to dynamical dissociation [15]. A suppression of the J/ψ yield in heavy-ion collisions relative to proton–proton collisions was observed at the SPS [16, 17], RHIC [18–21] and LHC [22–31]. However, at LHC energies, the J/ψ suppression is significantly reduced compared to lower energy results, in particular at low transverse momentum (p_T) and in more central collisions. These findings are interpreted by considering an additional contribution to the J/ψ production, known as regeneration, according to which the abundantly produced charm and anti-charm quarks from different hard partonic scatterings can recombine to form charmonium states [32, 33]. Previous ALICE inclusive J/ψ measurements at both central and forward rapidity, which have revealed significantly less suppression of J/ψ at low transverse momentum compared to lower energies [27, 28, 31] as well as non-zero elliptic flow [34, 35], have clearly demonstrated the relevance of this mechanism.

Different phenomenological scenarios are assumed for the description of charmonium production in heavy-ion collisions. In the Statistical Hadronisation model [32, 36], the abundances of all charmonium states are determined by thermal weights at the chemical freeze-out. By contrast, according to several partonic transport models [33, 37, 38] the charmonium states can be produced via regeneration throughout the full evolution of the QGP phase. Recent inclusive J/ψ results in Pb–Pb collisions at $\sqrt{s_{\text{NN}}} = 5.02\text{ TeV}$ indicate that both approaches can provide a description of the measured suppression within uncertainties in the low- p_T region [27, 28, 31]. Results of $\psi(2S)$ suppression recently released by the ALICE collaboration [39] show that transport models better reproduce charmonium measurements for central events compared to the Statistical Hadronisation model. Besides providing a good description of the production, transport models are also able to describe the elliptic flow of inclusive J/ψ [34, 40]. As the p_T of the J/ψ increases, the contribution from regeneration becomes less relevant, while charmonium dissociation and fragmentation of high-energy partons into charmonia become dominant.

Inclusive J/ψ production in high-energy hadronic collisions consists of several contributions: the J/ψ produced directly and from the decays of higher mass charmonium states (e.g. $\psi(2S)$ or χ_c), known as the “prompt” contribution, and J/ψ originating from the weak decays of beauty hadrons. The latter component, referred to as “non-prompt”, is characterised by a production vertex displaced with respect to the primary vertex of the collision, and this feature is exploited experimentally to separate the two contributions. The measurement of prompt J/ψ production enables a direct comparison with prompt charmonium models. In addition, the non-prompt J/ψ production measurement grants a direct insight into the suppression of beauty hadrons, which are expected to be sensitive to the properties of the medium created in heavy-ion collisions as ancestor beauty quarks experience energy loss by interacting with QGP constituents. The energy loss of partons inside the medium is expected to happen via both radiative [41, 42] and elastic collisional processes [43–45]. The relative contribution of the former is expected to increase with p_T . The energy loss strongly depends on the colour charge of the parton, being larger for gluons than for quarks, as well as on the parton mass [46–48]. The production of open heavy-flavour hadrons in nuclear collisions is also affected by in-medium hadronisation effects. Due to the high quark density in the QGP, heavy quarks can also hadronise via coalescence, by recombining with other light

flavour quarks inside the medium [49–51].

In order to interpret both prompt and non-prompt J/ ψ results in nuclear collisions, cold nuclear matter (CNM) effects need to be considered. The main effect at LHC energies is represented by the modification of the parton distribution functions of protons and neutrons inside nuclei compared to the ones of the free nucleons [52]. These effects are usually addressed through measurements in proton–nucleus collisions at the same centre-of-mass energy and are expected to be effective below 3 GeV/c for prompt J/ ψ , as shown by recent J/ ψ results in p–Pb collisions at $\sqrt{s_{\text{NN}}} = 5.02$ TeV [53]. For non-prompt J/ ψ , a small suppression with no significant p_{T} dependence is observed, although with large uncertainties [53].

At LHC energies in heavy-ion collisions, the production of prompt and non-prompt J/ ψ was measured at midrapidity by the CMS [22] and ALICE [54] collaborations in Pb–Pb collisions at $\sqrt{s_{\text{NN}}} = 2.76$ TeV. At the centre-of-mass energy of $\sqrt{s_{\text{NN}}} = 5.02$ TeV in the central rapidity region, the ATLAS [29] and CMS [30] collaborations measured the suppression of prompt and non-prompt J/ ψ at high transverse momentum. At low p_{T} , inclusive J/ ψ measurements were carried out by the ALICE collaboration [28, 31]. In this article, p_{T} and centrality dependent measurements of prompt and non-prompt J/ ψ production at midrapidity in Pb–Pb collisions at $\sqrt{s_{\text{NN}}} = 5.02$ TeV are presented. These results, obtained down to $p_{\text{T}} = 1.5$ GeV/c, have a unique kinematic coverage at the LHC compared to existing midrapidity measurements at the same centre-of-mass energy, which are available only at high transverse momentum. Furthermore, they have a significantly improved precision compared to previous published ALICE results at lower energy.

This article is organised as follows: the ALICE apparatus and data samples are described in Section 2, the analysis technique is presented in Section 3, results and comparison with similar measurements from other experiments and model calculations are discussed in Section 4, and finally the summary is provided in Section 5.

2 Experimental apparatus and data sample

The ALICE detector consists of a central barrel with a pseudorapidity coverage of $|\eta| < 0.9$ and a forward rapidity muon spectrometer with a pseudorapidity coverage for muons of $-4 < \eta < -2.5$. It also includes forward and backward pseudorapidity detectors employed for triggering, background rejection, and event characterisation. Central barrel detectors are placed inside a magnetic field $B = 0.5$ T provided by a solenoidal magnet. A complete description of the detector and an overview of its performance are discussed in Refs. [55, 56]. The main detectors employed for the analysis described in this article are the Inner Tracking System (ITS) [56], the Time Projection Chamber (TPC) [57] and the V0 detector [58]. Both ITS and TPC detectors enable the measurement of inclusive J/ ψ mesons via the dielectron decay channel in the central rapidity region down to zero p_{T} . The ITS consists of six layers of silicon detectors, with the two innermost layers composed of silicon pixel detectors (SPD) which provide the spatial resolution to separate prompt and non-prompt J/ ψ on a statistical basis. The TPC is the main tracking detector of the central barrel. In addition, it allows for particle identification via the measurement of the specific ionisation energy loss dE/dx in the detector gas. The V0 detector consists of two scintillator arrays placed on each side of the interaction point (with pseudorapidity coverage $2.8 < \eta < 5.1$ and $-3.7 < \eta < -1.7$), and it is used to reject offline beam-induced background events, to define a minimum bias trigger, and to characterise the event centrality. The zero degree calorimeters [59], located at ± 112.5 m on both sides of the interaction point, are used to reject electromagnetic interactions and beam-induced background in Pb–Pb collisions. The results presented in this article are based on the same data samples of Pb–Pb collisions at $\sqrt{s_{\text{NN}}} = 5.02$ TeV employed for the inclusive J/ ψ analysis [31]. In particular, it consist of a combination of the data samples collected during the years 2015 and 2018 of the LHC Run 2. In order to obtain a uniform acceptance of the detectors, only events with a reconstructed primary vertex position along the beam line located within ± 10 cm from the centre of the detector were

considered. In addition, consecutive events triggered within a time interval smaller than the readout time of the TPC were discarded as these are expected to have a high total charge deposition in the active volume and consequently significantly worse particle identification performance of the TPC. The datasets are collected with a minimum bias triggered event sample, provided by the coincidence of signals in the two scintillator arrays of the V0 detector. The corresponding integrated luminosity is about $24 \mu\text{b}^{-1}$ [60]. In addition, centrality triggered samples, whose trigger definition is based on the amplitude of the signal collected in the V0 detector, were used. These correspond to central (0–10%) and semicentral (30–50%) events, equivalent to an integrated luminosity of 105 and $51 \mu\text{b}^{-1}$ [60], respectively.

3 Data analysis

In order to estimate hot nuclear matter effects, the nuclear modification factor can be defined as the production yield in Pb–Pb collisions at $\sqrt{s_{\text{NN}}} = 5.02$ TeV normalised to the reference production cross section in pp collisions at the same energy and scaled by the average nuclear overlap function $\langle T_{\text{AA}} \rangle$ [60]:

$$R_{\text{AA}} = \frac{dN/dp_{\text{T}}dy}{\langle T_{\text{AA}} \rangle \times d\sigma_{\text{pp}}/dp_{\text{T}}dy}. \quad (1)$$

Inclusive J/ ψ measurements with no separation between prompt and non-prompt contributions are carried out by the ALICE collaboration at midrapidity ($|y| < 0.9$) in Pb–Pb collisions at $\sqrt{s_{\text{NN}}} = 5.02$ TeV, as discussed in Ref. [31]. The nuclear modification factors of prompt and non-prompt J/ ψ at midrapidity can be obtained by combining inclusive J/ ψ R_{AA} measurements with non-prompt J/ ψ fractions (f_{B}), the latter defined as the ratios of the production yields of J/ ψ mesons originating from beauty-hadron decays to that of inclusive J/ ψ , estimated in both Pb–Pb collisions and pp collisions at the same centre-of-mass energy.

3.1 Non-prompt J/ ψ analysis in Pb–Pb collisions

Selection of J/ ψ candidates

The event selection and track quality requirements used in the analysis discussed in this article are identical to those used for the corresponding midrapidity inclusive J/ ψ R_{AA} analysis in Pb–Pb collisions at $\sqrt{s_{\text{NN}}} = 5.02$ TeV [31]. Prompt and non-prompt J/ ψ measurements are carried out in the J/ ψ transverse momentum interval 1.5–10 GeV/c and in four different centrality classes, namely 0–10%, 10–30%, 30–50%, and 50–90%. The results are presented as a function of the transverse momentum of the J/ ψ , as well as of the average number of participants ($\langle N_{\text{part}} \rangle$). The latter can be estimated via Glauber model calculations [61–64] for the different centrality intervals [60].

J/ ψ candidates are reconstructed at midrapidity ($|y| < 0.9$) through the dielectron decay channel. Electron candidates, reconstructed using both ITS and TPC detectors, are required to have a pseudorapidity in the interval $|\eta| < 0.9$, a minimum transverse momentum of 1 GeV/c, and a minimum of 70 space points out of a maximum of 159 in the TPC. A hit in at least one of the two SPD layers is also required to improve the tracking and the spatial resolution. Several quality selection criteria, also employed for the inclusive J/ ψ analysis [31], are considered in order to ensure good track resolution, as well as to reduce the contribution of electrons and positrons originating from photon conversion in the detector material and to reject secondary tracks originating from weak decays. The electron identification relies on the measurement of dE/dx in the TPC, using stricter requirements than those considered for the inclusive J/ ψ analysis in order to increase the signal-to-background ratio, in particular at low transverse momentum and in central events. For tracks reconstructed in more peripheral centrality classes, namely 30–50% and 50–90%, the TPC dE/dx signal is required to lie within the interval $[-3, 3]\sigma_e$ relative to the expectation for electrons, where σ_e represents the specific energy-loss resolution for electrons in the TPC. In

addition, tracks consistent with the pion and proton assumptions within 3.5σ are rejected. For the centrality classes 0–10% and 10–30%, the electron inclusion is requested to be $[-2, 3]\sigma_e$ ($[-1, 3]\sigma_e$) for the p_T of the electron below (above) 5 GeV/c. A 4.5σ rejection for protons and pions is applied only below 5 GeV/c of the electron momentum at the inner wall of the TPC, while above 5 GeV/c the rejection is not applied to avoid reductions in the electron reconstruction efficiency. J/ ψ candidates are then obtained by considering all opposite-sign charged electron pairs. In 0–10% most central collisions, only candidates where both electron decay tracks have a hit in the first layer of the SPD are considered to optimise both the spatial resolution and signal-to-background ratio. For other centrality classes as well as in the highest p_T interval (7–10 GeV/c) in the 0–10% centrality class, where the signal-to-background ratio is better, the condition is released to increase the efficiency. Pair candidates where neither of the decay products has a hit in the first layer of the SPD are excluded due to the poor resolution of the secondary vertex.

Separation of prompt and non-prompt J/ ψ

The measurement of the non-prompt J/ ψ fraction is obtained through an unbinned two-dimensional likelihood fit procedure applied to reconstructed J/ ψ candidate pairs, following the same techniques employed in previous publications [53, 54, 65–67]. A simultaneous unbinned log-likelihood fit of the J/ ψ candidate distribution as a function of invariant mass (m_{ee}) and pseudoproper decay length (x) values is performed. The pseudoproper decay length is defined as $x = c \times L_{xy} \times m_{J/\psi}/p_T$, where $L_{xy} = (\vec{L} \times \vec{p}_T)/p_T$ represents the projection in the transverse plane of the vector pointing from the primary vertex to the J/ ψ decay vertex (\vec{L}) and $m_{J/\psi}$ is the J/ ψ mass provided by the Particle Data Group (PDG) [68]. The fit procedure maximises the logarithm of a likelihood function

$$\ln \mathcal{L} = \sum_{i=1}^N \ln [f_{\text{Sig}} \times F_{\text{Sig}}(x^i) \times M_{\text{Sig}}(m_{ee}^i) + (1 - f_{\text{Sig}}) \times F_{\text{Bkg}}(x^i) \times M_{\text{Bkg}}(m_{ee}^i)], \quad (2)$$

where N is the number of J/ ψ candidates within the invariant mass interval $2.72 < m_{ee} < 3.40$ GeV/c 2 ($2.60 < m_{ee} < 3.60$ GeV/c 2) in the centrality interval 0–10% (10–90%). A tighter invariant mass window is considered in most central collisions in order to increase the signal-to-background ratio in the fitting region, but still with a large enough sample of candidates to constrain the background probability density functions (PDFs). The relative amount of signal candidates, both prompt and non-prompt J/ ψ , with respect to the total number of candidates is quantified by the fit parameter f_{Sig} . The PDFs entering in Eq. 2, namely $F_{\text{Sig}}(x)$ and $F_{\text{Bkg}}(x)$ ($M_{\text{Sig}}(x)$ and $M_{\text{Bkg}}(x)$), are used to describe the pseudoproper decay length (invariant mass) distributions of signal and background, respectively. The pseudoproper decay length PDF of the signal is defined as

$$F_{\text{Sig}}(x) = f'_B \times F_B(x) + (1 - f'_B) \times F_{\text{prompt}}(x), \quad (3)$$

where $F_B(x)$ and $F_{\text{prompt}}(x)$ are the x PDFs for non-prompt and prompt J/ ψ , respectively, while f'_B represents the fraction of J/ ψ originating from beauty-hadron decays in the sample of selected dielectron candidates. Both f'_B and f_{Sig} are left as free parameters in the fitting procedure. A correction to the f'_B fraction obtained from the fit is applied to take into account the different average acceptance-times-efficiencies of prompt and non-prompt J/ ψ , which is a consequence of two effects: (i) different J/ ψ p_T distributions inside the wide p_T intervals where the measurements are provided; (ii) different J/ ψ polarisation, which can modify angular distributions of decay products and thus the J/ ψ acceptance. The corrected fraction of non-prompt J/ ψ , f_B , is obtained as

$$f_B = \left(1 + \frac{1 - f'_B}{f'_B} \times \frac{\langle A \times \epsilon \rangle_B}{\langle A \times \epsilon \rangle_{\text{prompt}}} \right)^{-1}, \quad (4)$$

where $\langle A \times \epsilon \rangle_{\text{prompt}}$ and $\langle A \times \epsilon \rangle_B$ represent the average acceptance-times-efficiency values for prompt and non-prompt J/ ψ , respectively, in the considered p_T interval. The functional forms of the different PDFs in Eq. 2 are determined either based on data or on Monte Carlo (MC) simulations, and are computed using the same procedures as in previous analyses [53, 54, 65, 66]. The PDFs corresponding to the signal component, namely $F_{\text{prompt}}(x)$, $F_B(x)$, and $M_{\text{Sig}}(m_{ee})$, as well as acceptance-times-efficiency corrections of prompt and non-prompt J/ ψ in Eq. 4, are determined from MC simulations. These simulations consist of prompt and non-prompt J/ ψ meson signals embedded in a background sample of Pb–Pb collisions at $\sqrt{s_{\text{NN}}} = 5.02$ TeV produced with HIJING [69]. The intervals of centrality for the Pb–Pb collisions considered in MC simulations are the same as those selected in experimental data. The prompt J/ ψ component is simulated with a p_T spectrum based on existing inclusive J/ ψ Pb–Pb measurements at midrapidity, while PYTHIA 6.4 [70] is used to generate beauty hadrons for non-prompt J/ ψ simulations. The decays of beauty hadrons into final states containing a J/ ψ meson are handled by the EvtGen R01-03-00 [71] package, while the J/ ψ decay into the dielectron channel is performed using the EvtGen package coupled with the PHOTOS model [72] for the treatment of radiative decays ($J/\psi \rightarrow e^+e^-\gamma$). Prompt J/ ψ are assumed to be unpolarised, while for the non-prompt J/ ψ a small residual polarisation as predicted by EvtGen [71] is considered. No further assumptions on the polarisation of both components are accounted, considering that existing measurements indicate small or no polarisation [73, 74]. The particle transport through the ALICE apparatus is handled by GEANT3 [75], considering a detailed description of the detector material and geometry. Detector responses and calibrations in MC simulations are tuned to data, taking into account time-dependent running conditions of all detectors included in the data acquisition.

The p_T spectrum of prompt J/ ψ in simulations is tuned to match experimentally observed distributions, taking into account the centrality dependence. In particular, the fits to measured inclusive J/ ψ yields from earlier publications [28, 31] are considered. To propagate the associated experimental uncertainties to the systematic uncertainties on acceptance-times-efficiency, all possible variations of the p_T shape within the envelope obtained by varying the fitting parameters according to their uncertainties are also considered. For non-prompt J/ ψ , different hypotheses are considered for the p_T distributions, including or excluding shadowing or suppression effects predicted by model calculations, such as those discussed in Sec. 4. Taking into account all hypotheses discussed above for prompt and non-prompt J/ ψ p_T spectra, an average correction factor for f'_B is evaluated. As the acceptance-times-efficiency corrections are weakly dependent on p_T , the resulting correction applied on f'_B according to Eq. 4 is small, being $\sim 5\%$ for the p_T integrated case, while for the different p_T intervals it ranges between 1% to 3%, depending on the width of the interval.

The resolution function, $F_{\text{prompt}}(x)$ in Eq. 3, defines the accuracy of x in the reconstruction, and affects all different PDFs related to the pseudoproper decay length. It is described by the sum of two Gaussians and a symmetric power law function. It is determined as a function of both p_T and centrality from MC simulations. A tuning procedure is applied in MC simulations to minimise the residual discrepancy with respect to data in the average distance of closest approach (DCA) of the track to the reconstructed interaction vertex in a plane perpendicular to the beam direction. A small centrality dependence is found for the x resolution, in particular the RMS of the resolution function changes by about 5% across different centrality classes, getting worse towards more central collisions. For the non-prompt J/ ψ , the pseudoproper decay length distribution $F_B(x)$ is modelled by the kinematic distribution of J/ ψ from beauty-hadron decays obtained from the MC simulation described above, and convoluted with the resolution function. Finally, MC simulations are also employed to determine the shape of the invariant mass signal $M_{\text{Sig}}(m_{ee})$, which is parametrised using a Crystal Ball function [76]. Background PDFs, for both invariant mass and pseudoproper decay length distributions, are built from data. The invariant mass background shape $M_{\text{Bkg}}(m_{ee})$, parametrised by a third order polynomial function, is estimated using the event-mixing technique, already used for the inclusive J/ ψ analysis at midrapidity [31], which also takes into account the residual background originating from correlated semileptonic decays of heavy-flavour

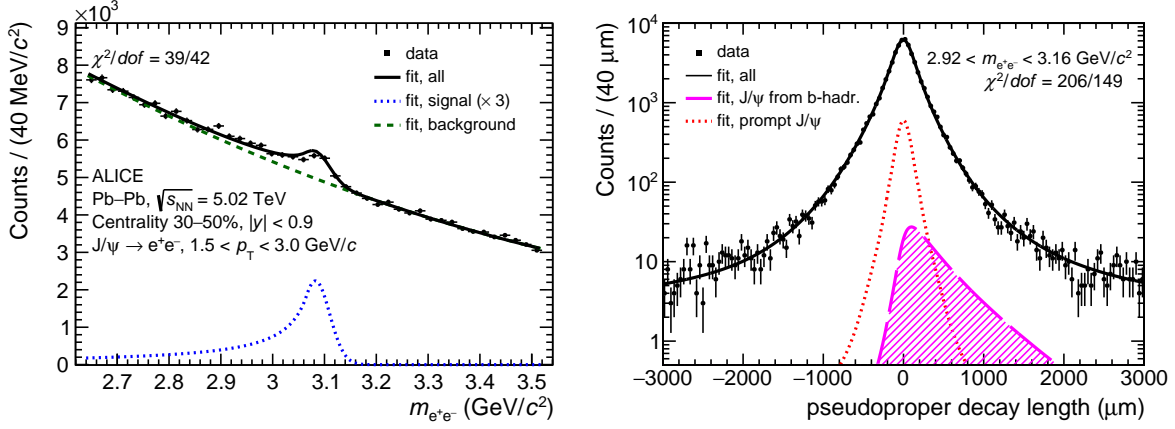


Figure 1: Invariant mass (left panel) and pseudoproper decay length (right panel) distributions of J/ψ candidates with maximum likelihood fit projections superimposed. The distributions in the figures correspond to selected candidates with $1.5 < p_{\text{T}} < 3.0 \text{ GeV}/c$ in the centrality class 30–50%. The pseudoproper decay length distribution is shown for J/ψ candidates reconstructed under the J/ψ mass peak, i.e. for $2.92 < m_{\text{ee}} < 3.16 \text{ GeV}/c^2$, for display purposes only. The χ^2 values, obtained by comparing the binned distributions of data points and the corresponding projections of the total fit function, are also reported.

hadrons. For the pseudoproper decay length background function, $F_{\text{Bkg}}(x)$, the same functional form and

Table 1: Invariant mass and p_{T} intervals considered for the definition of $F_{\text{Bkg}}(x)$ in different centrality classes (see text for details).

Centrality class	m_{ee} sidebands (GeV/c^2)	p_{T} intervals (GeV/c)
0–10%	2.72–2.8, 2.8–2.9, 3.2–3.3, 3.3–3.4	1.5–3, 3–5, 5–7, 7–10
10–30%, 30–50%, 50–90%	2.64–2.75, 2.75–2.85, 3.2–3.35, 3.35–3.52	1.5–3, 3–5, 5–10

strategy described in Ref. [54] is used. The function is determined for each centrality class by a fit to the data in four invariant mass regions on the sidebands of the J/ψ mass peak and in different p_{T} intervals, as summarised in Table 1. In each p_{T} interval, the x background function in the invariant mass region which contains the nominal J/ψ mass value is obtained by an interpolation procedure as the weighted combination of the PDFs determined in the other four invariant mass regions. The weights are chosen inversely proportional to the absolute or squared difference between the mean of the invariant mass distribution in the given mass interval and that in the interpolated region. Both hypotheses for the weights are considered for the study of the systematic uncertainty on the pseudoproper decay length background PDF. Additionally, the internal edges that define the invariant mass windows in Table 1 are shifted by $\pm 20 \text{ MeV}/c^2$, either in the same or opposite directions, and the interpolation procedure inside the signal region is repeated. For each p_{T} interval, a total of 9 (variations of mass intervals) \times 2 (linear or quadratic weights) = 18 attempts are obtained for $F_{\text{Bkg}}(x)$, which are used in turn in the unbinned likelihood fit procedure to determine f'_B . As the choice of a specific definition of mass intervals is in principle arbitrary, the central value of f'_B is computed considering the average of all the different attempts. Figure 1 shows an example of invariant mass (left panel) and pseudoproper decay length (right panel) distributions, corresponding to the centrality class 30–50% and transverse momentum range $1.5 < p_{\text{T}} < 3.0 \text{ GeV}/c$, with superimposed projections of the total maximum likelihood fit functions. The non-prompt J/ψ fraction is measured in four (three) p_{T} intervals in the centrality class 0–10% (10–30% and 30–50%), as well as in the p_{T} integrated case ($1.5 < p_{\text{T}} < 10 \text{ GeV}/c$) in the centrality classes 0–10%, 10–30%, 30–50%, and 50–90%.

Table 2: Systematic uncertainties on f_B , expressed in %, for the p_T integrated case, as well as for the lowest and the highest p_T interval in each centrality class.

p_T (GeV/c)	Cent. 0–10%			Cent. 10–30%			Cent. 30–50%			Cent. 50–90%
	1.5–10	1.5–3	7–10	1.5–10	1.5–3	5–10	1.5–10	1.5–3	5–10	1.5–10
Resolution function	2.5	5.0	1.0	3.5	5.0	1.0	2.5	3.5	1.0	2.5
x PDF of background	11.0	15.0	5.0	6.0	14.0	5.0	5.0	8.0	3.0	4.0
MC p_T distribution	6.0	1.5	3.0	6.0	1.5	4.0	6.0	1.5	3.0	6.0
x PDF of non-prompt J/ ψ	2.0	2.0	1.5	2.0	4.0	1.0	2.0	2.5	1.0	3.0
m_{ee} PDF of signal	0.5	1.5	0.5	0.5	0.5	0.5	0.5	0.5	0.5	0.5
m_{ee} PDF of background	0.5	2.5	0.5	1.0	2.5	0.5	0.5	1.5	0.5	0.5
Total	13.0	16.3	6.1	9.6	15.3	6.6	8.5	9.3	4.5	8.2

Systematic uncertainties

The systematic uncertainties on the measured non-prompt J/ ψ fractions in different p_T intervals and centrality classes are summarised in Table 2. Most of the contributions are due to the incomplete knowledge of the different PDFs of m_{ee} and x in the likelihood fit. An additional contribution originates from the assumptions of the p_T distributions of J/ ψ used in simulations, the latter particularly relevant for the p_T integrated case.

The dominant uncertainty is represented by the PDF of the pseudoproper decay length background, especially towards low p_T and more central collisions. Other contributions which become dominant in some cases are those originating from the resolution function, in particular in the lowest p_T intervals of each centrality, and the assumptions of the p_T distributions of J/ ψ used in simulations, the latter particularly relevant for the p_T integrated case.

The uncertainty on the resolution function is computed by considering the residual mismatch between data and MC simulations observed on the single track DCA resolution after the tuning procedure. The RMS of the resolution function is changed accordingly and the relative variation on f_B is taken as systematic uncertainty. The corresponding values are found to be larger at low p_T due to the worse pseudoproper decay length resolution and weakly dependent on centrality.

The uncertainty due to the pseudoproper decay length background PDF is estimated by computing the RMS of non-prompt J/ ψ fraction values obtained after changing the $F_{Bkg}(x)$ in the likelihood fit, considering the eighteen attempts previously mentioned, which depend on the choice of the m_{ee} sidebands. The uncertainty on f_B due to the $F_{Bkg}(x)$ is the major contribution, especially at low- p_T and more central collisions where the signal-to-background ratio gets worse.

The systematic uncertainty related to the p_T distributions of prompt and non-prompt J/ ψ mesons in MC simulations, mainly affecting the acceptance-times-efficiency correction on f_B according to Eq. 4, is evaluated by varying the prompt and non-prompt J/ ψ p_T shape considering the variations previously discussed in this section. Taking into account all combinations, an average correction factor for f'_B is evaluated, while the maximum variation with respect to the average value is used to estimate the corresponding systematic uncertainty. This contribution increases for wider p_T intervals, reaching about 6% for the p_T integrated interval, and is relatively independent of centrality.

To quantify the systematic uncertainty related to the shape of the x PDF of non-prompt J/ ψ , the p_T distribution of non-prompt J/ ψ is changed according to the same hypotheses considered for the estimate of the systematic uncertainty on the $\langle A \times \epsilon \rangle$ correction on f_B . Furthermore, the systematic uncertainty of the non-prompt J/ ψ x PDF originating from the description of the $h_b \rightarrow J/\psi + X$ decay kinematic, with h_b representing any beauty mesons or baryons, is evaluated by considering PYTHIA 6.4 instead of EvtGen for decaying beauty hadrons. For both EvtGen and PYTHIA, all default decay modes of beauty hadrons available in the corresponding package and including a J/ ψ in the final state, are considered.

The uncertainty on the invariant mass PDF of the J/ ψ signal is evaluated by changing the width of the Crystal Ball function in order to vary the fraction of candidates within the signal interval $2.92 < m_{ee} <$

Table 3: Fraction of non-prompt J/ψ with the corresponding uncertainties in pp collisions at $\sqrt{s} = 5.02$ TeV, obtained through the interpolation procedure, in different p_T intervals (see text for details).

p_T (GeV/ c)	f_B^{pp} at $\sqrt{s} = 5.02$ TeV
1.5–10	0.183 ± 0.004
1.5–3	0.110 ± 0.007
3–5	0.142 ± 0.004
5–7	0.190 ± 0.003
7–10	0.257 ± 0.005
5–10	0.227 ± 0.004

$3.16 \text{ GeV}/c^2$ by $\pm 2.5\%$. The latter variation corresponds to the systematic uncertainty on the MC signal shape assigned in the inclusive J/ψ analysis [31].

The uncertainty related to the invariant mass background PDF is evaluated by taking the maximum variation obtained for f_B after using in the likelihood fit procedure alternative functions, namely fourth and fifth order polynomial functions, for fitting the event mixing based distribution used for the determination of $M_{\text{Bkg}}(x)$.

The overall systematic uncertainty on f_B reaches a maximum of about 16% in the lowest p_T interval and in 0–10% centrality class, mostly as a consequence of both the increasing combinatorial background in more central collisions and the worsening of the x resolution at low transverse momenta.

3.2 Non-prompt J/ψ fractions in pp collisions at $\sqrt{s} = 5.02$ TeV

In pp collisions at $\sqrt{s} = 5.02$ TeV, non-prompt J/ψ fractions are measured at midrapidity by the ALICE collaboration [67] down to $p_T = 2$ GeV/ c . However, as the corresponding uncertainties are large and the p_T intervals in pp collisions do not match those of the Pb–Pb measurements, the p_T -differential f_B fractions are obtained via an interpolation procedure, already used in previous p–Pb and Pb–Pb analyses [53, 54, 65, 66]. This procedure is based on available non-prompt J/ψ fraction measurements in pp and $p\bar{p}$ collisions at midrapidity at several centre-of-mass energies, namely $\sqrt{s} = 1.96$ TeV (CDF [77]), 5.02 TeV (ALICE [67], CMS [78]), 7 TeV (ALICE [79], ATLAS [80, 81], CMS [82]) and 8 TeV (ATLAS [80]). In particular, using the semi-phenomenological function described in Ref. [54], which employs FONLL to describe the non-prompt J/ψ production cross section, the non-prompt J/ψ fraction in pp collisions at $\sqrt{s} = 5.02$ TeV (f_B^{pp}) as a function of p_T , needed for the computation of the reference for prompt and non-prompt $J/\psi R_{\text{AA}}$ measurements, is derived via an energy interpolation. The average f_B^{pp} in each p_T interval considered in the Pb–Pb analysis is obtained by reweighting the p_T -differential f_B^{pp} values by the inclusive p_T -differential J/ψ cross section in pp collisions at $\sqrt{s} = 5.02$ TeV [83].

The values of f_B^{pp} in the p_T intervals considered in the Pb–Pb analysis are summarised in Table 3. The uncertainty, which amounts to about 6.5% in the lowest p_T interval and decreases to about 1.5% at higher p_T , includes the contribution from experimental data and FONLL predictions, as well as the systematic uncertainty due to the choice of the functional form assumed for the energy interpolation (namely linear, exponential, and power law function).

4 Results and discussion

4.1 Non-prompt J/ψ fractions and J/ψ yields

The non-prompt J/ψ fraction measured by the ALICE collaboration in 0–10% Pb–Pb collisions as a function of p_T in $|y| < 0.9$ is shown in the left hand panel of Fig. 2. It is compared with similar results obtained by the ATLAS collaboration [29] at midrapidity, and available for p_T above 9.5 GeV/ c . In the right hand panel, the p_T -differential non-prompt J/ψ fractions measured by the ALICE collaboration

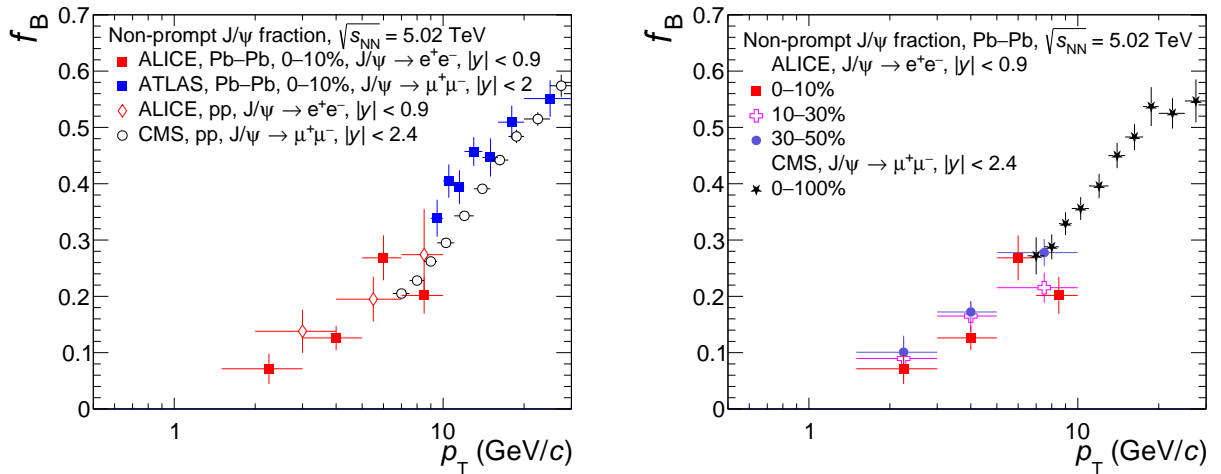


Figure 2: Non-prompt J/ ψ fraction as a function of transverse momentum measured by the ALICE collaboration in 0–10% most central Pb–Pb collisions (left panel) and in all centrality classes (right panel). Results in the left panel are compared with ATLAS midrapidity measurements [29] in the centrality class 0–10%, and with ALICE [67] and CMS [30] measurements in pp collisions at $\sqrt{s} = 5.02$ TeV. The ALICE measurements in the right panel are compared with similar midrapidity measurements from CMS [30], performed in the centrality class 0–100%. In both panels, the error bars represent the quadratic sum of statistical and systematic uncertainties.

in different centrality classes are compared with CMS results [30] available for $p_T > 6.5$ GeV/c in the centrality class 0–100%. The ALICE results complement the existing high- p_T measurements from ATLAS and CMS, matching the decreasing trend observed from high towards low p_T . The results in the centrality interval 0–10% suggest a smaller f_B compared to other centralities, in particular at low transverse momentum. In the left panel, non-prompt J/ ψ fraction measurements in pp collisions at $\sqrt{s} = 5.02$ TeV obtained by the ALICE [67] and CMS [30] collaborations are also shown for comparison, and exhibit a trend similar to the one observed in Pb–Pb collisions. In the p_T range 10 to 20 GeV/c, the non-prompt J/ ψ fractions are clearly higher in Pb–Pb compared to pp collisions, possibly suggesting a stronger nuclear suppression of prompt charmonia compared to beauty hadrons. On the other hand, at low- p_T results in the two systems exhibit similar values within uncertainties.

Figure 3 presents the non-prompt J/ ψ fraction as a function of centrality, expressed in terms of the average number of participants $\langle N_{\text{part}} \rangle$, measured by ALICE in Pb–Pb collisions at $\sqrt{s_{NN}} = 5.02$ TeV in the transverse momentum interval $1.5 < p_T < 10$ GeV/c. Within uncertainties, no centrality dependence is observed between peripheral and semicentral collisions, while the measured f_B in 0–10% most central collisions decreases in comparison to an average value computed by considering all other centralities with a significance of about 2.5σ considering both statistical and systematic uncertainties. This is consistent with the observations for the p_T -dependent results shown in Fig. 2 and is compatible with the hypothesis of a strong contribution of prompt J/ ψ originating from regeneration, which is expected to be larger in central compared to peripheral collisions. Current results are compared with earlier ALICE measurements based on Pb–Pb collisions at $\sqrt{s_{NN}} = 2.76$ TeV [54]. The statistical precision is significantly improved thanks to the larger event sample available from LHC Run 2. In the same figure, the p_T -integrated non-prompt J/ ψ fraction in pp collisions at $\sqrt{s} = 5.02$ TeV obtained by the interpolation procedure described in Section 3.2 is also shown. The corresponding value is found to be comparable with the non-prompt J/ ψ fractions measured in peripheral and semicentral Pb–Pb collisions.

The p_T -differential production yields of prompt and non-prompt J/ ψ in a given centrality interval are computed by combining the non-prompt J/ ψ fractions with the measured yields of inclusive J/ ψ [31], $dN^{\text{incl. } J/\psi}/dydp_T$, as

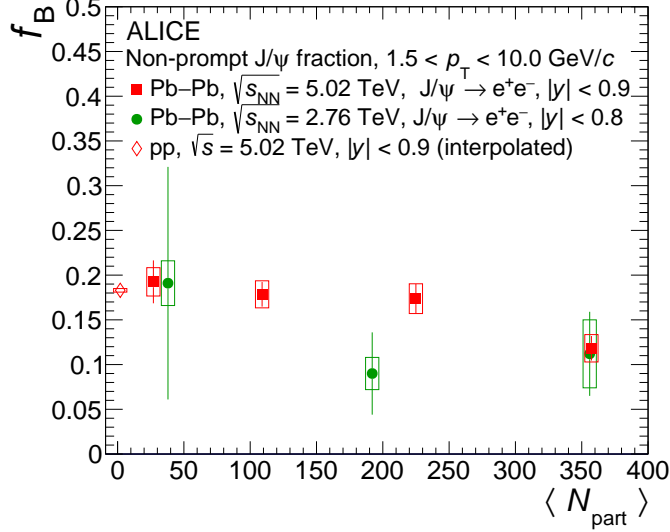


Figure 3: Centrality dependence (expressed in terms of average number of participants) of the non-prompt J/ ψ fraction measured by ALICE in Pb–Pb collisions at $\sqrt{s_{\text{NN}}} = 5.02 \text{ TeV}$ in the transverse momentum interval $1.5 < p_{\text{T}} < 10 \text{ GeV}/c$. Results are compared with previous ALICE measurements performed in Pb–Pb collisions at $\sqrt{s_{\text{NN}}} = 2.76 \text{ TeV}$ [54]. The p_{T} -integrated non-prompt J/ ψ fraction in pp collisions at $\sqrt{s} = 5.02 \text{ TeV}$ obtained from an interpolation procedure (see text for details) is also shown. Statistical and systematic uncertainties are shown by error bars and boxes, respectively.

$$\frac{dN^{J/\psi \leftarrow h_B}}{dydp_T} = f_B \times \frac{dN^{\text{incl. } J/\psi}}{dydp_T}, \quad \frac{dN^{\text{prompt } J/\psi}}{dydp_T} = (1 - f_B) \times \frac{dN^{\text{incl. } J/\psi}}{dydp_T}. \quad (5)$$

Figure 4 shows the p_{T} -differential production yields of prompt and non-prompt J/ ψ in the centrality interval 0–10%. Statistical and systematic uncertainties on prompt and non-prompt J/ ψ yields are evaluated by adding in quadrature the corresponding uncertainties on f_B and inclusive J/ ψ yields, the latter discussed in detail in Ref. [31]. The statistical uncertainties of inclusive J/ ψ yields vary from about 5% to 10%, depending on the p_{T} and the centrality of the collision. Regarding the systematic uncertainty of the inclusive J/ ψ yield, it ranges within 10–12% (8–10%) in the centrality class 0–10% (30–50%) and shows no significant p_{T} dependence. The measurements from ALICE are compared with p_{T} -differential production yields obtained by the ATLAS collaboration [29], as well as with inclusive J/ ψ measurements performed by the ALICE collaboration [31]. As already observed for the non-prompt J/ ψ fraction, the ALICE measurements provide complementary p_{T} coverage to ATLAS results, and they extend the measurement down to $p_{\text{T}} = 1.5 \text{ GeV}/c$. In addition, the ALICE and ATLAS results are qualitatively compatible in the overlapping region and show similar slopes, which result in an overall smooth trend over the full p_{T} range. Given the relatively small non-prompt J/ ψ fraction below 10 GeV/c, the inclusive J/ ψ yield and that of the prompt J/ ψ , both measured by the ALICE collaboration, are found to be comparable. However, the inclusive J/ ψ yield is measured in finer p_{T} intervals and subtends a wider range in p_{T} .

4.2 J/ ψ nuclear modification factors

The nuclear modification factor R_{AA} of prompt and non-prompt J/ ψ is obtained by combining the R_{AA} of inclusive J/ ψ [31], with the non-prompt J/ ψ fractions measured in Pb–Pb collisions at $\sqrt{s_{\text{NN}}} = 5.02 \text{ TeV}$ normalised to those in pp collisions obtained at the same centre-of-mass energy through the interpolation procedure described in Section 3.2:

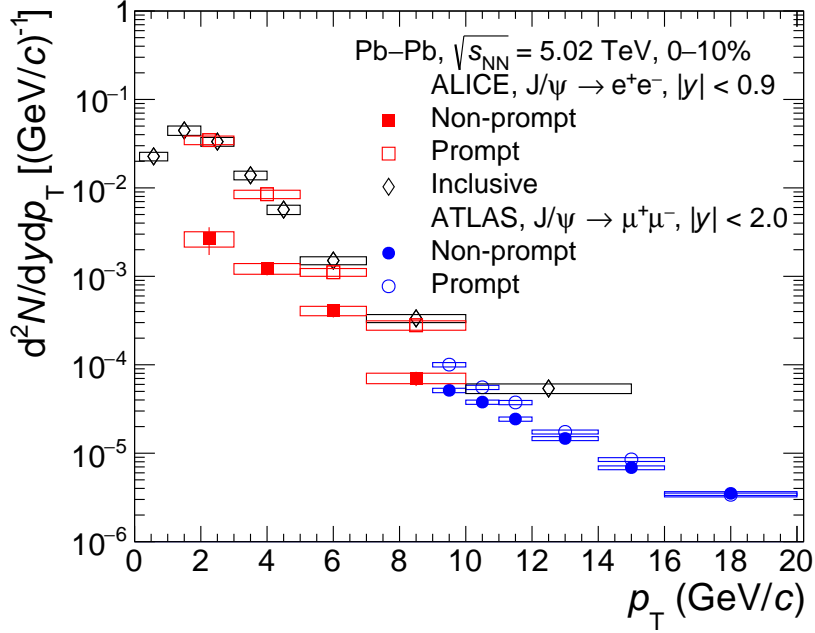


Figure 4: Prompt and non-prompt J/ ψ p_{T} -differential production yields measured by ALICE in the 0–10% centrality class at midrapidity, compared with similar measurements from the ATLAS collaboration [29] in the same centrality class. Inclusive J/ ψ yields measured by the ALICE collaboration in 0–10% [31] are shown for comparison. Error bars and boxes represent statistical and systematic uncertainties, respectively.

$$R_{\text{AA}}^{\text{J}/\psi \leftarrow h_B} = \frac{f_B^{\text{Pb-Pb}}}{f_B^{\text{pp}}} \times R_{\text{AA}}^{\text{inclusive J}/\psi}, \quad R_{\text{AA}}^{\text{prompt J}/\psi} = \frac{1 - f_B^{\text{Pb-Pb}}}{1 - f_B^{\text{pp}}} \times R_{\text{AA}}^{\text{inclusive J}/\psi}. \quad (6)$$

Statistical and systematic uncertainties on prompt and non-prompt J/ ψ R_{AA} are obtained by adding in quadrature the corresponding uncertainties on inclusive J/ ψ R_{AA} [31] and non-prompt J/ ψ fractions in Pb–Pb and in pp collisions, assuming all of them uncorrelated from each other. Uncertainties on inclusive J/ ψ R_{AA} , both statistical and systematic, include the corresponding contributions due to inclusive J/ ψ yields previously mentioned and inclusive J/ ψ cross section in pp collisions at $\sqrt{s} = 5.02$ TeV [83], the latter used as reference in the inclusive J/ ψ R_{AA} computation. The statistical uncertainty on the pp reference cross section increases with p_{T} from about 7% to 18%, while the systematic uncertainty is poorly dependent on p_{T} and it amounts to about 6%. The latter value do not include the normalisation uncertainty due to luminosity determination, which is 2.2% and it is considered within the global uncertainties when computing R_{AA} .

The p_{T} -differential nuclear modification factor of prompt J/ ψ is shown in Fig. 5 in different centrality classes, namely 0–10% (top left panel), 10–30% (top right panel) and 30–50% (bottom left panel). Global uncertainties, shown as boxes around unity, include correlated uncertainties on the pp reference due to normalisation as well as on the $\langle T_{\text{AA}} \rangle$ [31]. The latter uncertainty decreases with the collision centrality, varying from 0.7% in 0–10% most central collisions to 2% in the 50–90% centrality class. The R_{AA} of prompt J/ ψ in $1.5 < p_{\text{T}} < 10$ GeV/ c and as a function of centrality is shown in the bottom right panel of the same figure. The global uncertainty includes the contributions from the inclusive J/ ψ cross section and from f_B^{pp} in pp collisions, both integrated over p_{T} ($1.5 < p_{\text{T}} < 10$ GeV/ c). For $p_{\text{T}} > 5$ GeV/ c , the prompt J/ ψ R_{AA} in the centrality classes 10–30% and 30–50% reaches a value of about 0.4, while in 0–10% collisions it decreases to about 0.2, indicating a stronger suppression. The prompt J/ ψ R_{AA} increases towards low p_{T} and it exceeds unity in the lowest p_{T} interval (1.5–3 GeV/ c) of the 0–10% most central collisions. As a consequence, the p_{T} integrated prompt J/ ψ R_{AA} ($1.5 < p_{\text{T}} < 10$ GeV/ c) also

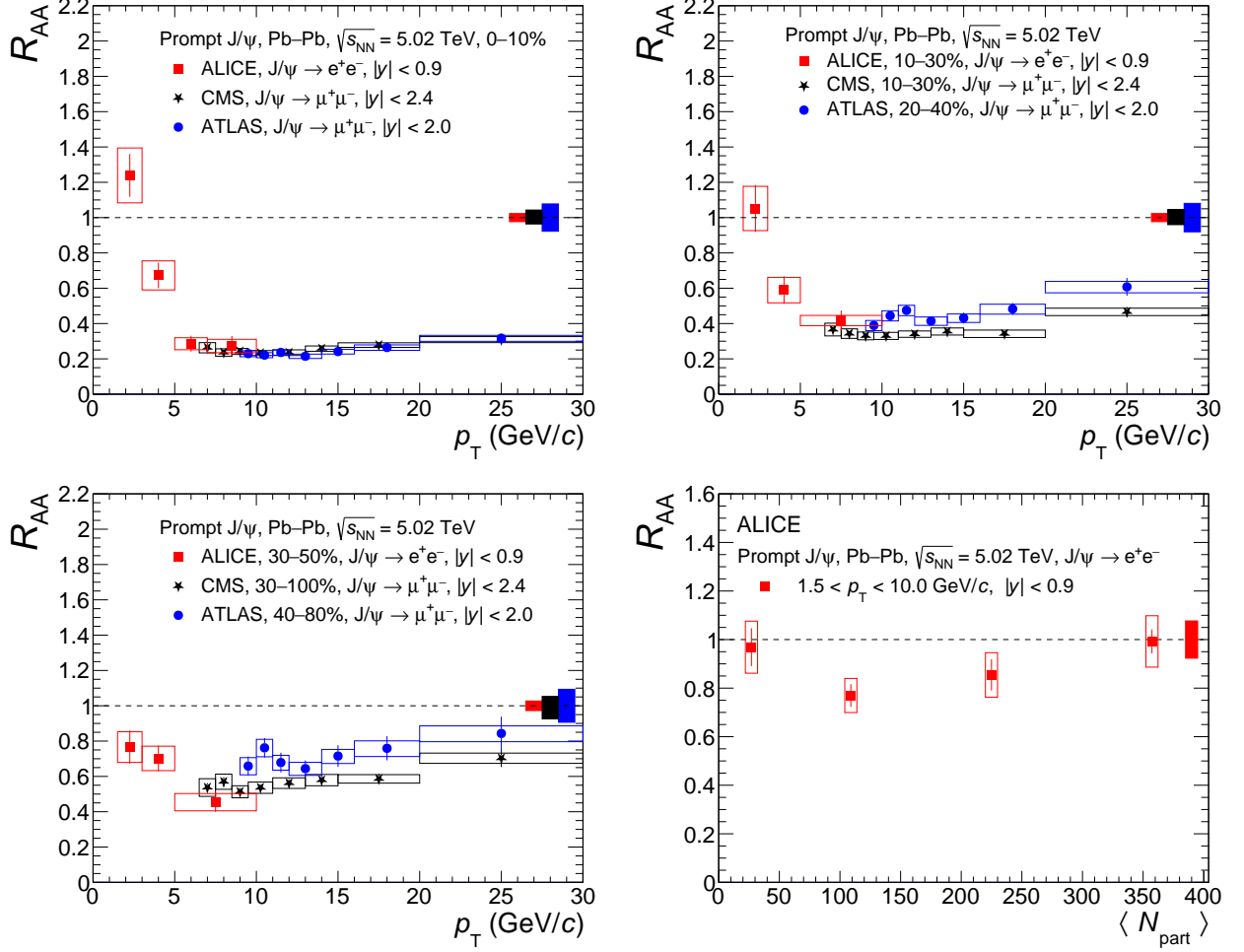


Figure 5: Nuclear modification factor of prompt J/ ψ as a function of p_T in 0–10% (upper left panel), 10–30% (top right panel) and 30–50% (bottom left panel) centrality classes. Results are compared with similar measurements from the ATLAS [29] and CMS [30] collaborations. The centrality dependent prompt J/ ψ R_{AA} in $1.5 < p_T < 10$ GeV/c is shown in the bottom right panel (centrality is expressed in terms of average number of participants). Error bars and boxes represent, respectively, statistical and systematic uncertainties uncorrelated with p_T (centrality, for the bottom right panel). Global uncertainties are shown as boxes around unity.

rises towards most central collisions, as shown in the bottom right panel of Fig. 5. According to prompt J/ ψ measurements performed by the ALICE collaboration in p–Pb collisions at $\sqrt{s_{\text{NN}}} = 5.02 \text{ TeV}$ [53], the R_{pPb} is found to be lower than unity within $1 < p_T < 3 \text{ GeV}/c$, suggesting significant CNM effects at play in Pb–Pb collisions in this transverse momentum region, while it becomes compatible with unity for $p_T > 3 \text{ GeV}/c$. The results from the ALICE collaboration are compared with similar measurements carried out by the ATLAS [29] and CMS [30] collaborations in the rapidity intervals $|y| < 2.0$ and $|y| < 2.4$, respectively. In the centrality interval 0–10%, the results from CMS and ATLAS are in good agreement with the ALICE measurements in the overlapping p_T interval, while in semicentral collisions the agreement is better with CMS than with ATLAS. It is worth noting that a smaller suppression for ATLAS measurements is expected in semicentral events, as the corresponding results use a significantly more peripheral collision sample compared to ALICE and CMS.

Figure 6 shows the nuclear modification factor of non-prompt J/ ψ as a function of p_T in the same centrality classes discussed previously for the prompt J/ ψ R_{AA} , namely 0–10%, 10–30% and 30–50%. The boxes around unity represent global uncertainties due to the normalisation of the pp reference cross section and $\langle T_{\text{AA}} \rangle$. Unlike the prompt J/ ψ R_{AA} , the p_T -differential nuclear modification factors of

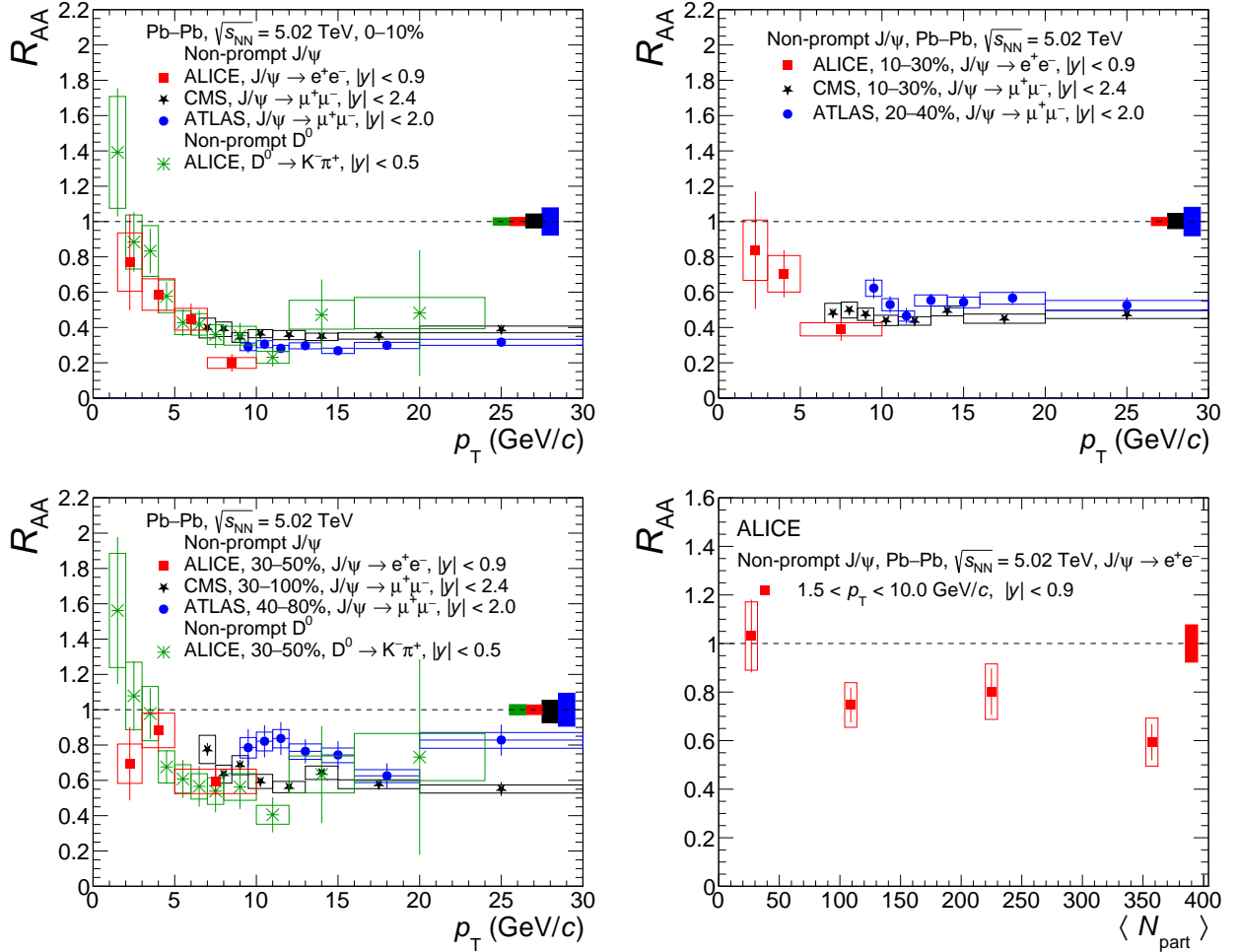


Figure 6: Nuclear modification factor of non-prompt J/ψ as a function of p_T in the 0–10% (upper left panel), 10–30% (top right panel) and 30–50% (bottom left panel). Results are compared with similar measurements from the ATLAS [29] and CMS [30] collaborations. Results in 0–10% and 30–50% are also compared to non-prompt D^0 R_{AA} measurements [84] in the same centrality classes. The centrality dependent non-prompt J/ψ R_{AA} in $1.5 < p_T < 10$ GeV/c is shown in the bottom right panel (centrality is expressed in terms of average number of participants). Error bars and boxes represent statistical and systematic uncertainties uncorrelated with p_T (centrality, for the bottom right panel). Global uncertainties are shown as boxes around unity.

non-prompt J/ψ are similar in the different centrality classes within experimental uncertainties below 5 GeV/c, while at higher p_T the suppression is larger in 0–10% most central collisions. The p_T -integrated R_{AA} in the bottom right panel of Fig. 6 hints at a decreasing trend towards more central collisions, reaching an R_{AA} value of about 0.6 in the 0–10% centrality class. In the case of non-prompt J/ψ , CNM effects are found to be small in the full measured p_T interval, as non-prompt J/ψ R_{pPb} measurements at $\sqrt{s_{NN}} = 5.02$ TeV [53] are everywhere compatible with unity, although uncertainties are large. Therefore, the observed modification can be attributed to the QGP formation in Pb–Pb collisions. Results as a function of p_T are shown together with non-prompt J/ψ R_{AA} measurements from the ATLAS [29] and CMS [30] collaborations, which are in good agreement with ALICE measurements in the overlapping p_T region. In 0–10% most central collisions, the R_{AA} from ALICE in the highest p_T interval shows a small tension of about 1.4σ and 2.5σ with respect to ATLAS and CMS, respectively. The non-prompt J/ψ R_{AA} measurements in 0–10% and 30–50% centrality classes are also compared with non-prompt D^0 results [84] measured at midrapidity by the ALICE collaboration. The results are compatible within uncertainties, despite possible differences that might originate from different decay kinematics of beauty hadrons to

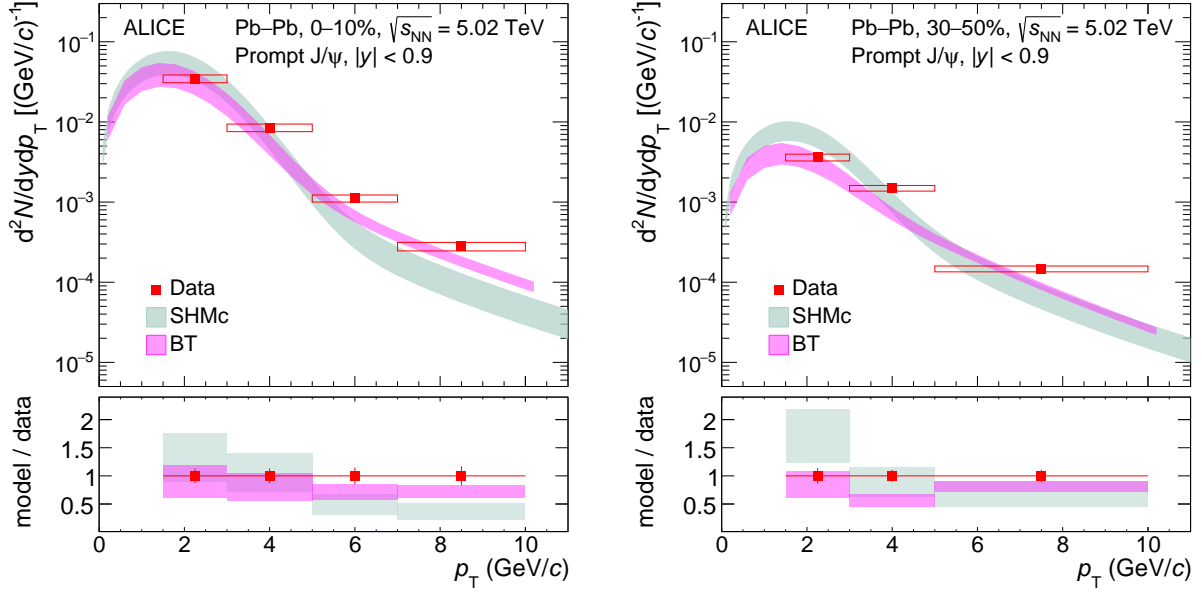


Figure 7: Prompt J/ ψ yields as a function of p_T in the 0–10% (left panel) and 30–50% (right panel) centrality classes compared with models [36, 37, 85]. Vertical error bars and boxes represent statistical and systematic uncertainties, respectively. Shaded bands in the top panels represent model uncertainties. Bottom panels show the ratios between models and data, with the bands representing the relative uncertainties of the models. Error bars around unity are the quadratic sum of statistical and systematic uncertainties on the measured yields.

J/ ψ and D⁰.

4.3 Comparison with models for prompt J/ ψ production

In the following, prompt J/ ψ measurements are compared with different phenomenological models in relativistic heavy-ion collisions.

Figure 7 shows the p_T -differential yields of prompt J/ ψ in the centrality classes 0–10% (left) and 30–50% (right), compared with different models, namely the statistical hadronisation model (SHMc) by Andronic *et al.* [36] and the Boltzmann transport model (BT) by Zhuang *et al.* [37, 85]. The bottom panels present the ratio of models to data, with the error bands representing the relative uncertainties originating from the models. For the computation of the ratio, an average value of the model is computed within the corresponding p_T intervals where the measurements are performed. Error bars around unity are the sum in quadrature of statistical and systematic uncertainties on the measured yields. In the SHMc model, the totality of charm quarks are produced in the initial hard parton–parton scatterings and thermalise inside the QGP. The total charm cross section employed in the SHMc calculations is the one measured by the ALICE collaboration in Pb–Pb collisions at $\sqrt{s_{NN}} = 5.02$ TeV, extracted from open-charm meson production measurements [84]. Effects from CNM are taken into account when calculating the total number of charm quarks in Pb–Pb using rapidity dependent measurements of the nuclear modification factor of D mesons in proton–nucleus collisions [86], where interpolations, if necessary, are done via model calculations. The yield of the different bound states is determined by thermal weights computed at a common chemical freeze-out. The relative abundances of open and hidden charm hadrons are determined using the equilibrium thermodynamical parameters obtained from fits to the measured yields of light-flavoured hadrons and D-mesons, with the latter being used to extract the charm fugacity. The spectra in the SHMc model are obtained by coupling the hadron yields with a modified blast-wave function with input from hydrodynamical calculations for the flow profiles [36]. In the BT model, the total charm cross section in Pb–Pb collisions is evaluated from the charm-production cross section measured in pp collisions [87] scaled by the number of binary collisions, while to estimate CNM effects the

EPS09 [88] gluon distributions are used. The dynamical evolution of the prompt charmonium states in the hot medium is described with a Boltzmann-type transport equation, including terms of dissociation and regeneration. The dissociation of charmonia inside the medium arises from the melting of the bound states due to colour Debye screening, as well as from collisional processes of charmonia with the medium constituents, and in particular from gluon dissociation. The regeneration cross section is connected to the dissociation cross section via the detailed balance between the gluon dissociation and reversed process. The model employs the (2+1)-dimensional version of the ideal hydrodynamic equations, including both a deconfined and a hadronic phase with a first order phase transition between these two. The uncertainties plotted in Fig. 7 for all models include contributions from total $c\bar{c}$ cross section, as well as uncertainties from CNM assumptions. Both SHMc and BT models show an overall good agreement with data within uncertainties, in particular for p_T below 5 GeV/c. At higher p_T , both models tend to underpredict the data, with the SHMc model showing a larger discrepancy, which is mainly due to the fact that in the SHMc model most of the produced J/ ψ yields are thermal, with only a small contribution from the collision corona.

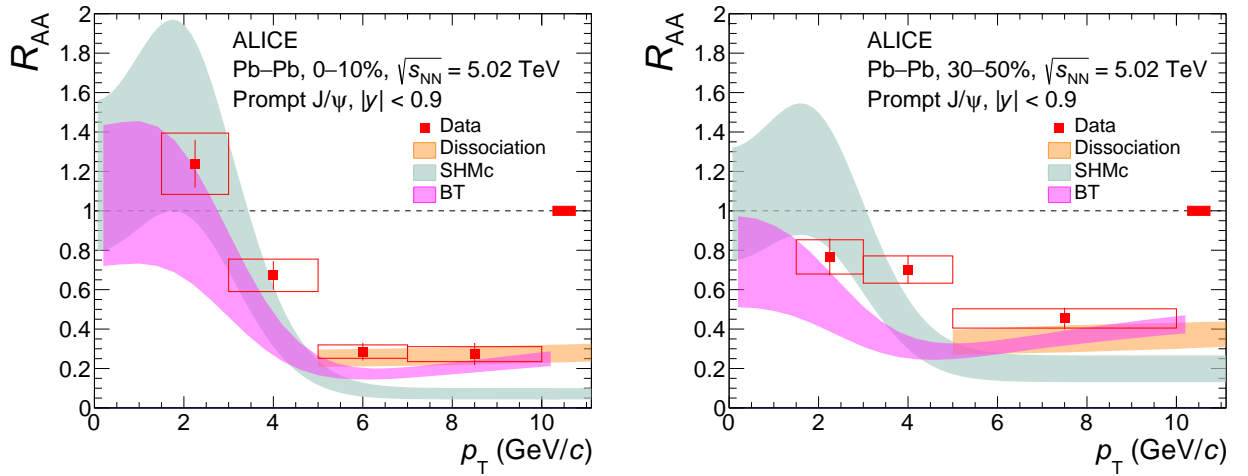


Figure 8: Prompt J/ ψ R_{AA} as a function of p_T in the 0–10% (left panel) and 30–50% (right panel) centrality classes compared with models [36, 37, 85, 89, 90]. Error bars and boxes represent statistical and uncorrelated systematic uncertainties. Shaded bands represent model uncertainties. The global uncertainty is shown around unity.

Figure 8 presents the prompt J/ ψ nuclear modification factor as a function of p_T in the centrality class 0–10% (left panel) and 30–50% (right panel) compared with model calculations. In addition to the SHMc and BT models, prompt J/ ψ R_{AA} measurements are also compared with the dissociation model by Vitev *et al.* [89]. In this model, which employs rate equations, the collisional dissociation of charmonia includes thermal effects on the wave function due to the screening of the $c\bar{c}$ attractive potential from the free colour charges in the QGP. The medium is modelled by a (2+1)-dimensional viscous hydrodynamic model. Non-relativistic quantum chromodynamics (NRQCD) theory [91] is used to obtain the baseline nucleon–nucleon cross sections for charmonia and the p_T -dependent feed-down from excited states. As this model provides predictions for $p_T > 5$ GeV/c, the contribution from CNM effects is assumed to be negligible. The SHMc model reproduces the prompt J/ ψ R_{AA} results at low p_T in both centrality classes, while it is significantly below the data for $p_T > 5$ GeV/c. The BT model provides a good description of the measurements in the full p_T range in 0–10% most central collisions, while the model underpredicts the data in the centrality class 30–50%. The dissociation model, available only above 5 GeV/c, provides a good description of prompt J/ ψ R_{AA} measurements within uncertainties.

The centrality dependence of the p_T -integrated ($1.5 < p_T < 10$ GeV/c) R_{AA} of prompt J/ ψ is compared with calculations from BT model in Fig. 9. The BT model, which shows a rising trend with increasing

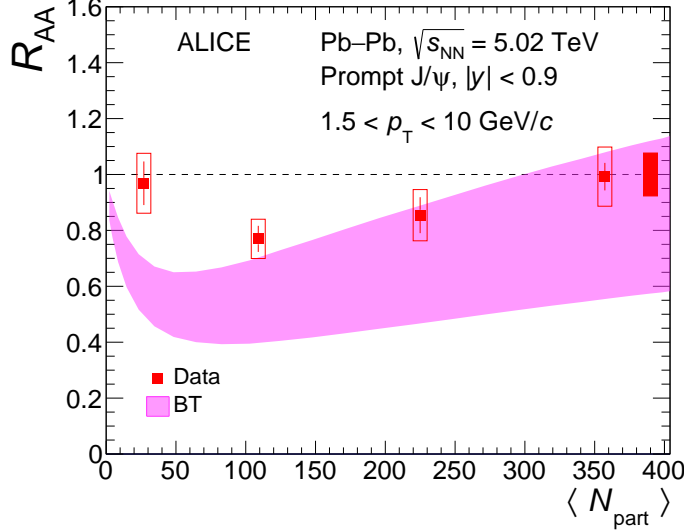


Figure 9: Centrality dependence (expressed in terms of average number of participants) of prompt J/ ψ R_{AA} measured by ALICE in Pb–Pb collisions at $\sqrt{s_{NN}} = 5.02$ TeV in the transverse momentum interval $1.5 < p_T < 10$ GeV/c. Results are compared with the BT model by Zhuang *et al.* [37, 85]. Error bars and boxes represent statistical and uncorrelated systematic uncertainties, respectively. Shaded bands represent model uncertainties. The global uncertainty is shown around unity.

number of participants from $\langle N_{\text{part}} \rangle \sim 50$, is in good agreement with experimental results in 0–10% and 10–30% centrality classes. Below $\langle N_{\text{part}} \rangle \sim 50$, both the data and the model exhibit a similar increasing trend towards more peripheral collisions, however the agreement between data and model worsens.

4.4 Comparison with models for non-prompt J/ ψ production

In the following, the comparison of non-prompt J/ ψ measurements with models describing open heavy-flavour production is discussed. As both the production mechanisms and the interaction with the medium are significantly different for prompt charmonia and open heavy-flavour hadrons, non-prompt J/ ψ measurements are compared with a different set of models with respect to those considered for prompt J/ ψ results.

In Fig. 10, the yields of non-prompt J/ ψ measured in the centralities 0–10% (left panel) and 30–50% (right panel), are compared with partonic transport model calculations [92–97]. The ratios of the models to data are depicted in the bottom panels, where the error bands are the model uncertainties. For computing the ratio, an average value of the model is considered within the corresponding p_T intervals where the measurements are performed. Error bars around unity are the quadratic sum of statistical and systematic uncertainties on the measured yields. In the transport model by Chen *et al.* [92] (LT1), as well as in the POWLANG transport model by Monteno *et al.* [93, 94], the Langevin equation is used for describing the evolution of the ancestor beauty quarks through the QGP. In POWLANG, transport coefficients are obtained either through perturbative calculations using the hard thermal loop (HTL) approach or calculations based on lattice QCD (LatQCD) simulations. The medium expansion is described by ideal (2+1)-dimensional hydrodynamic equations in LT1. In POWLANG, the background medium description is done via a (3+1)-dimensional hydrodynamic model, assuming no invariance for longitudinal boosts as considered in the (2+1)-dimensional case. The initial distribution of bottom quarks is parametrised according to perturbative-QCD calculations at fixed order with next-to-leading-log resummation (FONLL) [98] in LT1 and with the POWHEG-BOX package [99] in POWLANG. In both models, CNM effects are accounted for by using the EPS09 [88] gluon parton distribution functions, and at the hadronisation hypersurface, bottom and light-flavour quarks hadronise into beauty mesons

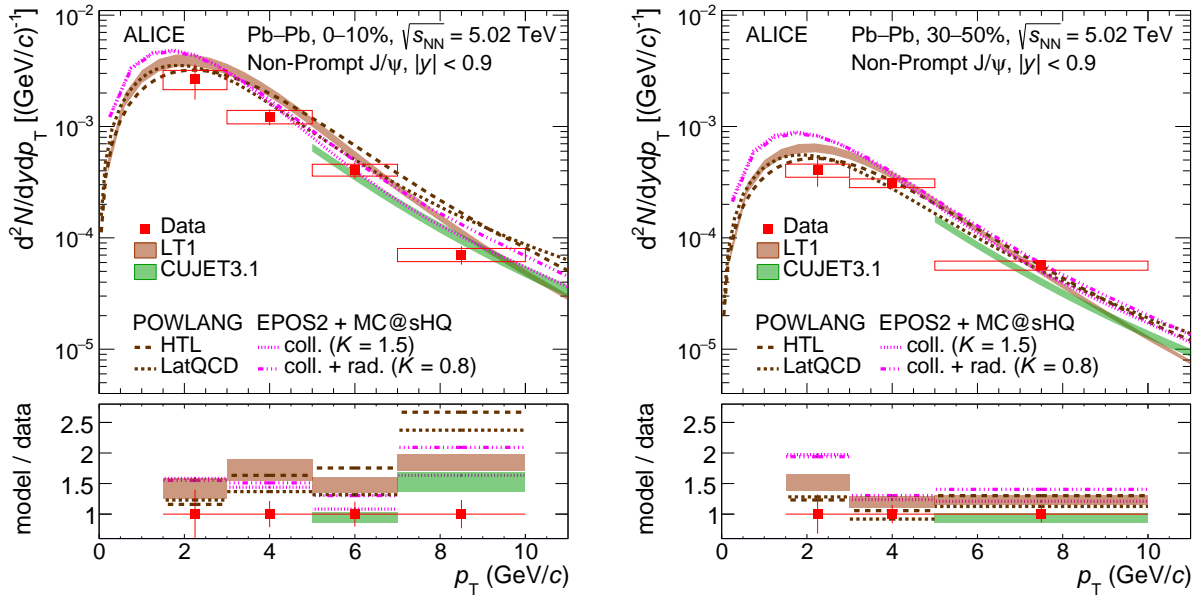


Figure 10: Non-prompt J/ ψ yields as a function of p_T in the 0–10% (left panel) and 30–50% (right panel) centrality classes compared with models [92–97]. Vertical error bars and boxes represent statistical and systematic uncertainties, respectively. Shaded bands in the top panels represent model uncertainties where applicable. Bottom panels show the ratios between models and data, with the bands representing the relative uncertainties from the models. Error bars around unity are the quadratic sum of statistical and systematic uncertainties on the measured yields.

via the coalescence model. In LT1, medium-induced gluon radiation is also included in the energy loss of heavy quarks, and becomes the dominant mechanism at large momentum, while in POWLANG the interactions of the heavy quarks with the medium constituents happen solely via collisional processes. In the calculations by Shi *et al.* [95, 96], the CUJET3.1 framework is used to evaluate the jet energy loss in a (2+1)-dimensional hydrodynamic background, implementing the contributions from collisional as well as from radiative processes. A set of R_{AA} and elliptic flow results from light hadrons in central and semicentral heavy-ion collisions is used to constrain the model, which is then used to predict heavy-flavour observables. For the initial p_T distribution of beauty quarks, FONLL calculations [98] with CTEQ6M [100] parton distribution functions are used. The formation of beauty hadrons happens via the classical vacuum-like fragmentation using the Peterson parametrisation in Ref. [101]. In the model by Gossiaux *et al.* [97] (EPOS2+MC@sHQ), the Monte Carlo treatment of the Boltzmann equation of heavy quarks (MC@sHQ) [102] is coupled to a (3+1)-dimensional fluid dynamical evolution of the locally thermalized QGP following the initial conditions from EPOS2 [103, 104]. The initial transverse momentum spectra of beauty quarks is obtained from FONLL calculations [98], and nuclear shadowing has been included according to the EPS09 [88] parametrization of the nuclear parton distribution functions. The calculations shown in this article consider two different configurations, either including pure collisional processes or both collisional and radiative ones. In order to further constrain the model, the corresponding cross sections are rescaled by a global factor K , which is chosen such that the predictions give a reasonable agreement at intermediate and high p_T with a set of D-meson R_{AA} measurements available in Pb–Pb collisions at $\sqrt{s_{NN}} = 2.76$ TeV [97]. In particular, $K = 0.8$ (1.5) is considered when both collisional and radiative (pure collisional) processes are included. After the evolution in the medium, the beauty quarks hadronize via both fragmentation and coalescence. The LT1, POWLANG and EPOS2+MC@sHQ models show systematically higher values compared to data, for both centrality classes in the full measured transverse momentum range. The discrepancy looks larger for POWLANG, especially in centrality class 0–10% and at higher p_T , which could be related to the absence of radiative processes in this model. The CUJET3.1 model, available only for p_T above 5 GeV/c, is compatible with

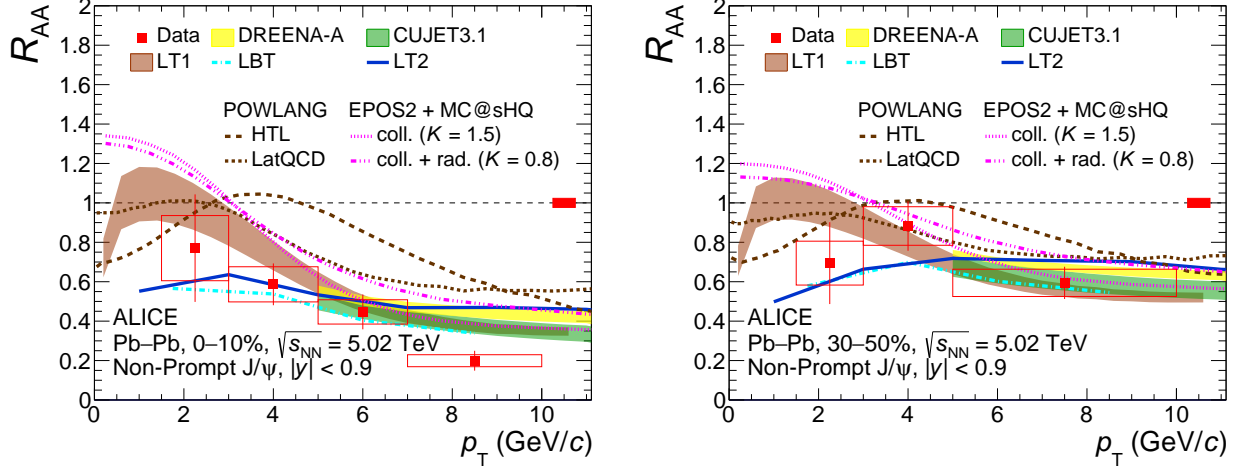


Figure 11: Non-prompt J/ ψ R_{AA} as a function of p_T in the 0–10% (left panel) and 30–50% (right panel) centrality classes compared with models [92, 95–97, 105–108]. Error bars and boxes represent statistical and uncorrelated systematic uncertainties, respectively. Shaded bands represent model uncertainties where applicable. The global uncertainty is shown around unity.

the data within uncertainties.

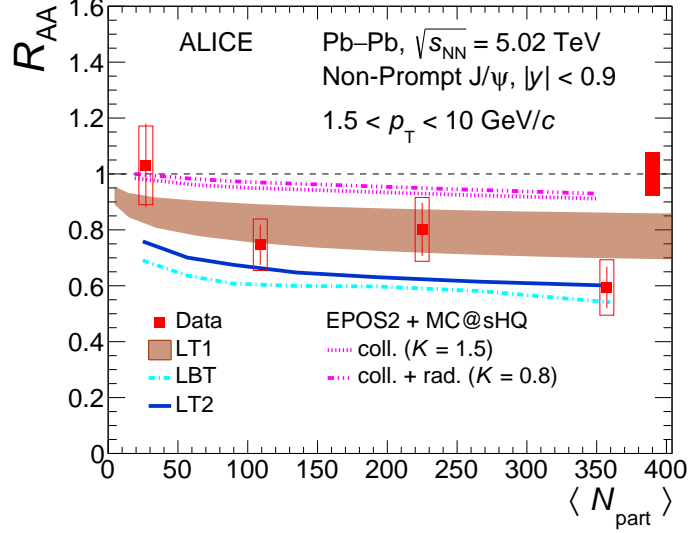


Figure 12: Centrality dependence (expressed in terms of average number of participants) of non-prompt J/ ψ R_{AA} measured by ALICE in Pb–Pb collisions at $\sqrt{s_{NN}} = 5.02$ TeV in the transverse momentum interval $1.5 < p_T < 10$ GeV/ c . Results are compared with several partonic transport models [92, 97, 105, 106]. Error bars and boxes represent statistical and uncorrelated systematic uncertainties, respectively. Shaded bands represent model uncertainties where applicable. The global uncertainty is shown around unity

The nuclear modification factor of non-prompt J/ ψ is compared with models in Fig. 11 in 0–10% (left panel) and 30–50% (right panel) centrality intervals. The results are compared with the LT1, CUJET3.1, POWLANG and EPOS2+MC@sHQ models previously described as well as with additional ones [105–108]. In these additional calculations, the space–time evolution of the QGP is simulated using a (3+1)-dimensional viscous hydrodynamic model and both collisional and radiative energy loss mechanisms inside a thermal medium are considered. In the calculation by Li *et al.* [105], marked as LT2, the interactions between heavy quarks and the QGP are described by an improved Langevin approach. The transport model by Xing *et al.* [106] employs an extended linear Boltzmann transport (LBT) equation,

which includes both short and long-range interactions of heavy quarks with the QGP. In both LT2 and LBT models, the initial heavy quark p_T distribution is simulated according to FONLL calculations using CT14NLO [109] parton distribution functions modified according to the EPPS16 [110] next-to-leading-order parametrisation, while beauty hadrons are produced through a hybrid fragmentation–coalescence model [111]. The calculation by Djordjevic *et al.* [107, 108] employs a framework (DREENA-A) which combines the state-of-the-art dynamical energy loss model with hydrodynamical simulations. The initial heavy-quark spectrum is computed using next-to-leading-order calculations described in Ref. [112] and KLP [113] fragmentation functions are used for the formation of beauty mesons. In both centralities all available model predictions except POWLANG show compatible values for p_T above 5 GeV/c, and within uncertainties are in an overall good agreement with the data. The POWLANG model overpredicts the R_{AA} in the centrality class 0–10% and at high p_T , which might be a consequence of the lack of radiative energy loss contributions in this model. Below 5 GeV/c, the LT1 and POWLANG models sit on the upper side of the data points in both centrality classes, still being compatible with them within uncertainties, while the EPOS2+MC@HQ model overpredicts the measurements. Both LBT and LT2 models are compatible with the measured R_{AA} within uncertainties in the full measured p_T range, and in both centrality classes.

Figure 12 depicts the non-prompt J/ ψ R_{AA} , integrated over p_T in the interval $1.5 < p_T < 10$ GeV/c, as a function of the number of participants in comparison with transport models. The LT1 model shows a slightly decreasing trend moving towards central collisions, and is compatible with data within uncertainties for all centrality classes. The LBT, LT2 and EPOS2+MC@HQ models predict a similar decreasing trend for the non-prompt J/ ψ R_{AA} towards larger $\langle N_{\text{part}} \rangle$. The LBT and LT2 models show good agreement with R_{AA} results in 0–10% centrality class, while for other centrality classes both models slightly underpredict the data. The EPOS2+MC@HQ model agrees with measured R_{AA} in the most peripheral class, while it tends to overestimate measurements towards more central collisions.

5 Summary

Prompt and non-prompt J/ ψ production is measured by the ALICE collaboration in Pb–Pb collisions at $\sqrt{s_{\text{NN}}} = 5.02$ TeV in the rapidity interval $|y| < 0.9$ as a function of p_T and centrality. In particular, p_T -differential measurements of non-prompt J/ ψ fractions, production yields, and nuclear modification factors are carried out. The ALICE results extend the existing CMS and ATLAS measurements at midrapidity, available only at high p_T , down to $p_T = 1.5$ GeV/c, and all measurements look compatible within uncertainties in the common p_T intervals. Non-prompt J/ ψ fractions show a rising trend with increasing p_T , similar to the one observed in pp collisions, while no significant dependence on the centrality is observed within uncertainties, with the exception of most central collisions where f_B exhibits a significant decrease with respect to other centrality classes. The comparison with earlier measurements in Pb–Pb collisions at $\sqrt{s_{\text{NN}}} = 2.76$ TeV shows compatible results at the two centre-of-mass energies and highlights a significantly improved precision with Run 2 data.

For $p_T > 5$ GeV/c, the prompt J/ ψ R_{AA} decreases with increasing centrality, while at lower p_T the suppression is smaller in 0–10% most central collisions, in particular in the lowest p_T interval where the prompt J/ ψ R_{AA} exceeds unity. These results are consistent with p_T -integrated measurements of prompt J/ ψ R_{AA} , which rises with $\langle N_{\text{part}} \rangle$, hinting at an increasing contribution from regeneration at low p_T and more central collisions. In 0–10% most central collisions, the SHMc model and transport microscopic calculations that include a contribution from regeneration are compatible with experimental data for $p_T < 5$ GeV/c. However, at higher p_T , transport models are compatible with the measurements within uncertainties, while the SHMc model significantly underpredicts the data. In semicentral collisions there is less agreement between data and models. In particular, for p_T above 3 GeV/c the models either underpredict the data or sit at the lower edge of the experimental uncertainty.

The non-prompt J/ ψ R_{AA} integrated over p_{T} hints at a decreasing trend towards more central collisions. As a function of p_{T} , the non-prompt J/ ψ R_{AA} in different centrality classes are compatible within uncertainties below 5 GeV/c, while at higher p_{T} the suppression is larger in the centrality interval 0–10%. Results are consistent within uncertainties with non-prompt D⁰ R_{AA} measurements in the centrality classes 0–10% and 30–50%. Several transport models are able to describe the data within uncertainties. All calculations, but POWLANG, implement both collisional and radiative energy loss processes combined with a dynamically expanding QGP, considering different hypotheses on transport dynamics, CNM effects, p_{T} distributions and hadronisation of beauty quarks. Above 5 GeV/c, all calculations predict a similar suppression for non-prompt J/ ψ and are consistent with the data within uncertainties, with the exception of POWLANG, which overpredicts the data in most central events. This points to the importance of radiative energy loss contributions in the high- p_{T} region. At lower p_{T} and for the p_{T} -integrated case, theoretical calculations predict different magnitudes of the suppression. However, due to the current precision of the measurements it is not possible to discriminate among them as all calculations are compatible with the data within uncertainties.

Both prompt and non-prompt J/ ψ measurements will improve significantly taking advantage of the larger expected data sample and the better spatial resolution provided at midrapidity by the upgraded ITS [114] in the next LHC runs. In particular, further differential measurements in the non-prompt charmonium sector, in addition to yet unmeasured observables such as the elliptic flow, could allow further constraining different open beauty hadron production models.

Acknowledgements

The ALICE Collaboration would like to thank all its engineers and technicians for their invaluable contributions to the construction of the experiment and the CERN accelerator teams for the outstanding performance of the LHC complex. The ALICE Collaboration gratefully acknowledges the resources and support provided by all Grid centres and the Worldwide LHC Computing Grid (WLCG) collaboration. The ALICE Collaboration acknowledges the following funding agencies for their support in building and running the ALICE detector: A. I. Alikhanyan National Science Laboratory (Yerevan Physics Institute) Foundation (ANSL), State Committee of Science and World Federation of Scientists (WFS), Armenia; Austrian Academy of Sciences, Austrian Science Fund (FWF): [M 2467-N36] and Nationalstiftung für Forschung, Technologie und Entwicklung, Austria; Ministry of Communications and High Technologies, National Nuclear Research Center, Azerbaijan; Conselho Nacional de Desenvolvimento Científico e Tecnológico (CNPq), Financiadora de Estudos e Projetos (Finep), Fundação de Amparo à Pesquisa do Estado de São Paulo (FAPESP) and Universidade Federal do Rio Grande do Sul (UFRGS), Brazil; Bulgarian Ministry of Education and Science, within the National Roadmap for Research Infrastructures 2020-2027 (object CERN), Bulgaria; Ministry of Education of China (MOEC) , Ministry of Science & Technology of China (MSTC) and National Natural Science Foundation of China (NSFC), China; Ministry of Science and Education and Croatian Science Foundation, Croatia; Centro de Aplicaciones Tecnológicas y Desarrollo Nuclear (CEADEN), Cubaenergía, Cuba; Ministry of Education, Youth and Sports of the Czech Republic, Czech Republic; The Danish Council for Independent Research | Natural Sciences, the VILLUM FONDEN and Danish National Research Foundation (DNRF), Denmark; Helsinki Institute of Physics (HIP), Finland; Commissariat à l’Energie Atomique (CEA) and Institut National de Physique Nucléaire et de Physique des Particules (IN2P3) and Centre National de la Recherche Scientifique (CNRS), France; Bundesministerium für Bildung und Forschung (BMBF) and GSI Helmholtzzentrum für Schwerionenforschung GmbH, Germany; General Secretariat for Research and Technology, Ministry of Education, Research and Religions, Greece; National Research, Development and Innovation Office, Hungary; Department of Atomic Energy Government of India (DAE), Department of Science and Technology, Government of India (DST), University Grants Commission, Government of India (UGC) and Council of Scientific and Industrial Research (CSIR), India; National

Research and Innovation Agency - BRIN, Indonesia; Istituto Nazionale di Fisica Nucleare (INFN), Italy; Japanese Ministry of Education, Culture, Sports, Science and Technology (MEXT) and Japan Society for the Promotion of Science (JSPS) KAKENHI, Japan; Consejo Nacional de Ciencia (CONACYT) y Tecnología, through Fondo de Cooperación Internacional en Ciencia y Tecnología (FONCICYT) and Dirección General de Asuntos del Personal Académico (DGAPA), Mexico; Nederlandse Organisatie voor Wetenschappelijk Onderzoek (NWO), Netherlands; The Research Council of Norway, Norway; Commission on Science and Technology for Sustainable Development in the South (COMSATS), Pakistan; Pontificia Universidad Católica del Perú, Peru; Ministry of Education and Science, National Science Centre and WUT ID-UB, Poland; Korea Institute of Science and Technology Information and National Research Foundation of Korea (NRF), Republic of Korea; Ministry of Education and Scientific Research, Institute of Atomic Physics, Ministry of Research and Innovation and Institute of Atomic Physics and University Politehnica of Bucharest, Romania; Ministry of Education, Science, Research and Sport of the Slovak Republic, Slovakia; National Research Foundation of South Africa, South Africa; Swedish Research Council (VR) and Knut & Alice Wallenberg Foundation (KAW), Sweden; European Organization for Nuclear Research, Switzerland; Suranaree University of Technology (SUT), National Science and Technology Development Agency (NSTDA), Thailand Science Research and Innovation (TSRI) and National Science, Research and Innovation Fund (NSRF), Thailand; Turkish Energy, Nuclear and Mineral Research Agency (TENMAK), Turkey; National Academy of Sciences of Ukraine, Ukraine; Science and Technology Facilities Council (STFC), United Kingdom; National Science Foundation of the United States of America (NSF) and United States Department of Energy, Office of Nuclear Physics (DOE NP), United States of America. In addition, individual groups or members have received support from: European Research Council, Strong 2020 - Horizon 2020 (grant nos. 950692, 824093), European Union; Academy of Finland (Center of Excellence in Quark Matter) (grant nos. 346327, 346328), Finland.

References

- [1] F. Karsch, “Lattice simulations of the thermodynamics of strongly interacting elementary particles and the exploration of new phases of matter in relativistic heavy ion collisions”, *J. Phys. Conf. Ser.* **46** (2006) 122–131, arXiv:hep-lat/0608003.
- [2] **Wuppertal-Budapest** Collaboration, S. Borsanyi, Z. Fodor, C. Hoelbling, S. D. Katz, S. Krieg, C. Ratti, and K. K. Szabo, “Is there still any T_c mystery in lattice QCD? Results with physical masses in the continuum limit III”, *JHEP* **09** (2010) 073, arXiv:1005.3508 [hep-lat].
- [3] S. Borsanyi, Z. Fodor, C. Hoelbling, S. D. Katz, S. Krieg, and K. K. Szabo, “Full result for the QCD equation of state with 2+1 flavors”, *Phys. Lett. B* **730** (2014) 99–104, arXiv:1309.5258 [hep-lat].
- [4] A. Bazavov *et al.*, “The chiral and deconfinement aspects of the QCD transition”, *Phys. Rev. D* **85** (2012) 054503, arXiv:1111.1710 [hep-lat].
- [5] T. Csorgo, “New form of matter at CERN SPS: Quark Matter but not Quark Gluon Plasma”, *Nucl. Phys. B Proc. Suppl.* **92** (2001) 62–74, arXiv:hep-ph/0011339.
- [6] D. Teaney, J. Lauret, and E. V. Shuryak, “Flow at the SPS and RHIC as a Quark Gluon Plasma signature”, *Phys. Rev. Lett.* **86** (2001) 4783–4786, arXiv:nucl-th/0011058.
- [7] **BRAHMS** Collaboration, I. Arsene *et al.*, “Quark Gluon Plasma and color glass condensate at RHIC? The Perspective from the BRAHMS experiment”, *Nucl. Phys. A* **757** (2005) 1–27, arXiv:nucl-ex/0410020.
- [8] **PHOBOS** Collaboration, B. B. Back *et al.*, “The PHOBOS perspective on discoveries at RHIC”, *Nucl. Phys. A* **757** (2005) 28–101, arXiv:nucl-ex/0410022.

- [9] **STAR** Collaboration, J. Adams *et al.*, “Experimental and theoretical challenges in the search for the Quark Gluon Plasma: The STAR Collaboration’s critical assessment of the evidence from RHIC collisions”, *Nucl. Phys. A* **757** (2005) 102–183, arXiv:nucl-ex/0501009.
- [10] **PHENIX** Collaboration, K. Adcox *et al.*, “Formation of dense partonic matter in relativistic nucleus-nucleus collisions at RHIC: Experimental evaluation by the PHENIX collaboration”, *Nucl. Phys. A* **757** (2005) 184–283, arXiv:nucl-ex/0410003.
- [11] **ALICE** Collaboration, “The ALICE experiment – A journey through QCD”, arXiv:2211.04384 [nucl-ex].
- [12] A. Andronic *et al.*, “Heavy-flavour and quarkonium production in the LHC era: from proton–proton to heavy-ion collisions”, *Eur. Phys. J. C* **76** (2016) 107, arXiv:1506.03981 [nucl-ex].
- [13] F.-M. Liu and S.-X. Liu, “Quark Gluon Plasma formation time and direct photons from heavy ion collisions”, *Phys. Rev. C* **89** (2014) 034906, arXiv:1212.6587 [nucl-th].
- [14] T. Matsui and H. Satz, “ J/ψ Suppression by Quark-Gluon Plasma Formation”, *Phys. Lett. B* **178** (1986) 416–422.
- [15] A. Rothkopf, “Heavy Quarkonium in Extreme Conditions”, *Phys. Rept.* **858** (2020) 1–117, arXiv:1912.02253 [hep-ph].
- [16] C. Baglin *et al.*, “ ψ' and J/ψ production in p-W, p-U and S-U interactions at 200 GeV/nucleon”, *Physics Letters B* **345** (1995) 617–621.
- [17] **NA50** Collaboration, B. Alessandro *et al.*, “A New measurement of J/ψ suppression in Pb-Pb collisions at 158-GeV per nucleon”, *Eur. Phys. J. C* **39** (2005) 335–345, arXiv:hep-ex/0412036.
- [18] **PHENIX** Collaboration, A. Adare *et al.*, “ J/ψ Production vs Centrality, Transverse Momentum, and Rapidity in Au+Au Collisions at $\sqrt{s_{NN}} = 200$ GeV”, *Phys. Rev. Lett.* **98** (2007) 232301, arXiv:nucl-ex/0611020.
- [19] **PHENIX** Collaboration, A. Adare *et al.*, “ J/ψ suppression at forward rapidity in Au+Au collisions at $\sqrt{s_{NN}} = 200$ GeV”, *Phys. Rev. C* **84** (2011) 054912, arXiv:1103.6269 [nucl-ex].
- [20] **STAR** Collaboration, B. Abelev *et al.*, “ J/ψ production at high transverse momentum in p+p and Cu+Cu collisions at $\sqrt{s_{NN}} = 200$ GeV”, *Phys. Rev. C* **80** (2009) 041902, arXiv:0904.0439 [nucl-ex].
- [21] **STAR** Collaboration, L. Adamczyk *et al.*, “ J/ψ production at low p_T in Au + Au and Cu + Cu collisions at $\sqrt{s_{NN}} = 200$ GeV with the STAR detector”, *Phys. Rev. C* **90** (2014) 024906, arXiv:1310.3563 [nucl-ex].
- [22] **CMS** Collaboration, S. Chatrchyan *et al.*, “Suppression of non-prompt J/ψ , prompt J/ψ , and $Y(1S)$ in PbPb collisions at $\sqrt{s_{NN}} = 2.76$ TeV”, *JHEP* **05** (2012) 063, arXiv:1201.5069 [nucl-ex].
- [23] **ALICE** Collaboration, B. Abelev *et al.*, “ J/ψ suppression at forward rapidity in Pb-Pb collisions at $\sqrt{s_{NN}} = 2.76$ TeV”, *Phys. Rev. Lett.* **109** (2012) 072301, arXiv:1202.1383 [hep-ex].

- [24] ALICE Collaboration, B. Abelev *et al.*, “Centrality, rapidity and transverse momentum dependence of J/ ψ suppression in Pb-Pb collisions at $\sqrt{s_{\text{NN}}}=2.76$ TeV”, *Phys. Lett. B* **734** (2014) 314–327, arXiv:1311.0214 [nucl-ex].
- [25] ALICE Collaboration, J. Adam *et al.*, “Differential studies of inclusive J/ ψ and $\psi(2S)$ production at forward rapidity in Pb-Pb collisions at $\sqrt{s_{\text{NN}}} = 2.76$ TeV”, *JHEP* **05** (2016) 179, arXiv:1506.08804 [nucl-ex].
- [26] ALICE Collaboration, J. Adam *et al.*, “J/ ψ suppression at forward rapidity in Pb-Pb collisions at $\sqrt{s_{\text{NN}}} = 5.02$ TeV”, *Phys. Lett. B* **766** (2017) 212–224, arXiv:1606.08197 [nucl-ex].
- [27] ALICE Collaboration, S. Acharya *et al.*, “Studies of J/ ψ production at forward rapidity in Pb-Pb collisions at $\sqrt{s_{\text{NN}}} = 5.02$ TeV”, *JHEP* **02** (2020) 041, arXiv:1909.03158 [nucl-ex].
- [28] ALICE Collaboration, S. Acharya *et al.*, “Centrality and transverse momentum dependence of inclusive J/ ψ production at midrapidity in Pb-Pb collisions at sNN=5.02 TeV”, *Phys. Lett. B* **805** (2020) 135434, arXiv:1910.14404 [nucl-ex].
- [29] ATLAS Collaboration, M. Aaboud *et al.*, “Prompt and non-prompt J/ ψ and $\psi(2S)$ suppression at high transverse momentum in 5.02 TeV Pb+Pb collisions with the ATLAS experiment”, *Eur. Phys. J. C* **78** (2018) 762, arXiv:1805.04077 [nucl-ex].
- [30] CMS Collaboration, A. M. Sirunyan *et al.*, “Measurement of prompt and nonprompt charmonium suppression in PbPb collisions at 5.02 TeV”, *Eur. Phys. J. C* **78** (2018) 509, arXiv:1712.08959 [nucl-ex].
- [31] ALICE Collaboration, S. Acharya *et al.*, “Measurements of inclusive J/ ψ production at midrapidity and forward rapidity in Pb–Pb collisions at $\sqrt{s_{\text{NN}}} = 5.02$ TeV”, *Phys. Lett. B* **849** (2024) 138451, arXiv:2303.13361 [nucl-ex].
- [32] P. Braun-Munzinger and J. Stachel, “(Non)thermal aspects of charmonium production and a new look at J/ ψ suppression”, *Phys. Lett. B* **490** (2000) 196–202, arXiv:nucl-th/0007059.
- [33] R. L. Thews, M. Schroedter, and J. Rafelski, “Enhanced j/ ψ production in deconfined quark matter”, *Phys. Rev. C* **63** (Apr, 2001) 054905.
- [34] ALICE Collaboration, S. Acharya *et al.*, “J/ ψ elliptic and triangular flow in Pb-Pb collisions at $\sqrt{s_{\text{NN}}} = 5.02$ TeV”, *JHEP* **10** (2020) 141, arXiv:2005.14518 [nucl-ex].
- [35] ALICE Collaboration, S. Acharya *et al.*, “J/ ψ elliptic flow in Pb-Pb collisions at $\sqrt{s_{\text{NN}}} = 5.02$ TeV”, *Phys. Rev. Lett.* **119** (2017) 242301, arXiv:1709.05260 [nucl-ex].
- [36] A. Andronic, P. Braun-Munzinger, M. K. Köhler, K. Redlich, and J. Stachel, “Transverse momentum distributions of charmonium states with the statistical hadronization model”, *Phys. Lett. B* **797** (2019) 134836, arXiv:1901.09200 [nucl-th].
- [37] K. Zhou, N. Xu, Z. Xu, and P. Zhuang, “Medium effects on charmonium production at ultrarelativistic energies available at the CERN Large Hadron Collider”, *Phys. Rev. C* **89** (2014) 054911, arXiv:1401.5845 [nucl-th].
- [38] X. Du and R. Rapp, “Sequential Regeneration of Charmonia in Heavy-Ion Collisions”, *Nucl. Phys. A* **943** (2015) 147–158, arXiv:1504.00670 [hep-ph].
- [39] ALICE Collaboration, “ $\psi(2S)$ suppression in Pb-Pb collisions at the LHC”, *Phys. Rev. Lett.* **132** (2024) 042301, arXiv:2210.08893 [nucl-ex].

- [40] M. He, H. van Hees, and R. Rapp, “Heavy-quark diffusion in the quark–gluon plasma”, *Prog. Part. Nucl. Phys.* **130** (2023) 104020, arXiv:2204.09299 [hep-ph].
- [41] M. Gyulassy and M. Plumer, “Jet Quenching in Dense Matter”, *Phys. Lett. B* **243** (1990) 432–438.
- [42] R. Baier, Y. L. Dokshitzer, A. H. Mueller, S. Peigne, and D. Schiff, “Radiative energy loss and p_T broadening of high-energy partons in nuclei”, *Nucl. Phys. B* **484** (1997) 265–282, arXiv:hep-ph/9608322.
- [43] M. H. Thoma and M. Gyulassy, “Quark damping and energy loss in the high temperature QCD”, *Nuclear Physics B* **351** (1991) 491–506.
- [44] E. Braaten and M. H. Thoma, “Energy loss of a heavy fermion in a hot QED plasma”, *Phys. Rev. D* **44** (Aug, 1991) 1298–1310.
- [45] E. Braaten and M. H. Thoma, “Energy loss of a heavy quark in the quark-gluon plasma”, *Phys. Rev. D* **44** (Nov, 1991) R2625–R2630.
- [46] Y. L. Dokshitzer and D. E. Kharzeev, “Heavy quark colorimetry of QCD matter”, *Phys. Lett. B* **519** (2001) 199–206, arXiv:hep-ph/0106202.
- [47] N. Armesto, C. A. Salgado, and U. A. Wiedemann, “Medium induced gluon radiation off massive quarks fills the dead cone”, *Phys. Rev. D* **69** (2004) 114003, arXiv:hep-ph/0312106.
- [48] S. Wicks, W. Horowitz, M. Djordjevic, and M. Gyulassy, “Heavy quark jet quenching with collisional plus radiative energy loss and path length fluctuations”, *Nucl. Phys. A* **783** (2007) 493–496, arXiv:nucl-th/0701063.
- [49] R. J. Fries, B. Muller, C. Nonaka, and S. A. Bass, “Hadronization in heavy ion collisions: Recombination and fragmentation of partons”, *Phys. Rev. Lett.* **90** (2003) 202303, arXiv:nucl-th/0301087.
- [50] L. Ravagli and R. Rapp, “Quark Coalescence based on a Transport Equation”, *Phys. Lett. B* **655** (2007) 126–131, arXiv:0705.0021 [hep-ph].
- [51] V. Greco, C. M. Ko, and R. Rapp, “Quark coalescence for charmed mesons in ultrarelativistic heavy ion collisions”, *Phys. Lett. B* **595** (2004) 202–208, arXiv:nucl-th/0312100.
- [52] N. Armesto, “Nuclear shadowing”, *J. Phys. G* **32** (2006) R367–R394, arXiv:hep-ph/0604108.
- [53] **ALICE** Collaboration, S. Acharya *et al.*, “Inclusive, prompt and non-prompt J/ ψ production at midrapidity in p–Pb collisions at $\sqrt{s_{\text{NN}}} = 5.02 \text{ TeV}$ ”, *JHEP* **06** (2022) 011, arXiv:2105.04957 [nucl-ex].
- [54] **ALICE** Collaboration, J. Adam *et al.*, “Inclusive, prompt and non-prompt J/ ψ production at mid-rapidity in Pb–Pb collisions at $\sqrt{s_{\text{NN}}} = 2.76 \text{ TeV}$ ”, *JHEP* **07** (2015) 051, arXiv:1504.07151 [nucl-ex].
- [55] **ALICE** Collaboration, K. Aamodt *et al.*, “The ALICE experiment at the CERN LHC”, *JINST* **3** (2008) S08002.
- [56] **ALICE** Collaboration, B. Abelev *et al.*, “Performance of the ALICE Experiment at the CERN LHC”, *Int. J. Mod. Phys. A* **29** (2014) 1430044, arXiv:1402.4476 [nucl-ex].
- [57] J. Alme *et al.*, “The ALICE TPC, a large 3-dimensional tracking device with fast readout for ultra-high multiplicity events”, *Nucl. Instrum. Meth. A* **622** (2010) 316 – 367, arXiv:1001.1950.

- [58] ALICE Collaboration, E. Abbas *et al.*, “Performance of the ALICE VZERO system”, *JINST* **8** (2013) P10016, arXiv:1306.3130 [nucl-ex].
- [59] ALICE Collaboration, P. Cortese, “Performance of the ALICE Zero Degree Calorimeters and upgrade strategy”, *J. Phys. Conf. Ser.* **1162** (2019) 012006.
- [60] ALICE Collaboration, “Centrality determination in heavy ion collisions”, ALICE-PUBLIC-2018-011 . <https://cds.cern.ch/record/2636623>.
- [61] R. J. Glauber and G. Matthiae, “High-energy scattering of protons by nuclei”, *Nucl. Phys. B* **21** (1970) 135–157.
- [62] M. L. Miller, K. Reygers, S. J. Sanders, and P. Steinberg, “Glauber modeling in high-energy nuclear collisions”, *Annual Review of Nuclear and Particle Science* **57** (2007) 205–243.
- [63] D. d’Enterria and C. Loizides, “Progress in the Glauber Model at Collider Energies”, *Ann. Rev. Nucl. Part. Sci.* **71** (2021) 315–344, arXiv:2011.14909 [hep-ph].
- [64] C. Loizides, J. Kamin, and D. d’Enterria, “Improved Monte Carlo Glauber predictions at present and future nuclear colliders”, *Phys. Rev. C* **97** (2018) 054910, arXiv:1710.07098 [nucl-ex]. [Erratum: Phys.Rev.C 99, 019901 (2019)].
- [65] ALICE Collaboration, S. Acharya *et al.*, “J/ ψ production at midrapidity in p–Pb collisions at $\sqrt{s_{\text{NN}}} = 8.16 \text{ TeV}$ ”, *JHEP* **07** (2023) 137, arXiv:2211.14153 [nucl-ex].
- [66] ALICE Collaboration, S. Acharya *et al.*, “Prompt and non-prompt J/ ψ production and nuclear modification at mid-rapidity in p–Pb collisions at $\sqrt{s_{\text{NN}}} = 5.02 \text{ TeV}$ ”, *Eur. Phys. J. C* **78** (2018) 466, arXiv:1802.00765 [nucl-ex].
- [67] ALICE Collaboration, S. Acharya *et al.*, “Prompt and non-prompt J/ ψ production cross sections at midrapidity in proton-proton collisions at $\sqrt{s} = 5.02$ and 13 TeV ”, *JHEP* **03** (2022) 190, arXiv:2108.02523 [nucl-ex].
- [68] Particle Data Group Collaboration, R. L. Workman and Others, “Review of Particle Physics”, *PTEP* **2022** (2022) 083C01.
- [69] X.-N. Wang and M. Gyulassy, “HIJING: A Monte Carlo model for multiple jet production in pp, pA, and AA collisions”, *Phys. Rev. D* **44** (Dec, 1991) 3501–3516.
- [70] T. Sjstrand, S. Mrenna, and P. Z. Skands, “PYTHIA 6.4 Physics and Manual”, *JHEP* **05** (2006) 026, arXiv:hep-ph/0603175.
- [71] D. Lange, “The EvtGen particle decay simulation package”, *Nucl. Instrum. Meth. A* **462** (2001) 152–155.
- [72] E. Barberio and Z. Was, “PHOTOS - a universal Monte Carlo for QED radiative corrections: version 2.0”, *Computer Physics Communications* **79** (1994) 291 – 308.
- [73] ALICE Collaboration, S. Acharya *et al.*, “Measurement of the inclusive J/ ψ polarization at forward rapidity in pp collisions at $\sqrt{s} = 8 \text{ TeV}$ ”, *Eur. Phys. J. C* **78** (2018) 562, arXiv:1805.04374 [hep-ex].
- [74] ALICE Collaboration, S. Acharya *et al.*, “First measurement of quarkonium polarization in nuclear collisions at the LHC”, *Phys. Lett. B* **815** (2021) 136146, arXiv:2005.11128 [nucl-ex].

- [75] R. Brun, F. Bruyant, F. Carminati, S. Giani, M. Maire, A. McPherson, G. Patrick, and L. Urban, *GEANT: Detector Description and Simulation Tool; Oct 1994*. CERN Program Library. CERN, Geneva, 1993. <https://cds.cern.ch/record/1082634>. Long Writeup W5013.
- [76] J. E. Gaiser, “Charmonium Spectroscopy From Radiative Decays of the J/ψ and ψ' ”, ph.d. thesis, 8, 1982. <https://inspirehep.net/literature/183554>.
- [77] **CDF** Collaboration, D. Acosta *et al.*, “Measurement of the J/ψ meson and b –hadron production cross sections in $p\bar{p}$ collisions at $\sqrt{s} = 1960$ GeV”, *Phys. Rev. D* **71** (2005) 032001, [arXiv:hep-ex/0412071](https://arxiv.org/abs/hep-ex/0412071).
- [78] **CMS** Collaboration, A. M. Sirunyan *et al.*, “Measurement of prompt and nonprompt J/ψ production in pp and pPb collisions at $\sqrt{s_{NN}} = 5.02$ TeV”, *Eur. Phys. J. C* **77** (2017) 269, [arXiv:1702.01462](https://arxiv.org/abs/1702.01462) [nucl-ex].
- [79] **ALICE** Collaboration, B. Abelev *et al.*, “Measurement of prompt J/ψ and beauty hadron production cross sections at mid-rapidity in pp collisions at $\sqrt{s} = 7$ TeV”, *JHEP* **11** (2012) 065, [arXiv:1205.5880](https://arxiv.org/abs/1205.5880) [hep-ex].
- [80] **ATLAS** Collaboration, G. Aad *et al.*, “Measurement of the differential cross-sections of prompt and non-prompt production of J/ψ and $\psi(2S)$ in pp collisions at $\sqrt{s} = 7$ and 8 TeV with the ATLAS detector”, *Eur. Phys. J. C* **76** (2016) 283, [arXiv:1512.03657](https://arxiv.org/abs/1512.03657) [hep-ex].
- [81] **ATLAS** Collaboration, G. Aad *et al.*, “Measurement of the differential cross-sections of inclusive, prompt and non-prompt J/ψ production in proton-proton collisions at $\sqrt{s} = 7$ TeV”, *Nucl. Phys. B* **850** (2011) 387–444, [arXiv:1104.3038](https://arxiv.org/abs/1104.3038) [hep-ex].
- [82] **CMS** Collaboration, A. Khachatryan *et al.*, “Prompt and Non-Prompt J/ψ Production in pp Collisions at $\sqrt{s} = 7$ TeV”, *Eur. Phys. J. C* **71** (2011) 1575, [arXiv:1011.4193](https://arxiv.org/abs/1011.4193) [hep-ex].
- [83] **ALICE** Collaboration, S. Acharya *et al.*, “Inclusive J/ψ production at mid-rapidity in pp collisions at $\sqrt{s} = 5.02$ TeV”, *JHEP* **10** (2019) 084, [arXiv:1905.07211](https://arxiv.org/abs/1905.07211) [nucl-ex].
- [84] **ALICE** Collaboration, S. Acharya *et al.*, “Measurement of beauty production via non-prompt D^0 mesons in Pb-Pb collisions at $\sqrt{s_{NN}} = 5.02$ TeV”, *JHEP* **12** (2022) 126, [arXiv:2202.00815](https://arxiv.org/abs/2202.00815) [nucl-ex].
- [85] B. Chen, “Thermal production of charmonia in Pb-Pb collisions at $\sqrt{s_{NN}} = 5.02$ TeV”, *Chin. Phys. C* **43** (2019) 124101, [arXiv:1811.11393](https://arxiv.org/abs/1811.11393) [nucl-th].
- [86] **LHCb** Collaboration, R. Aaij *et al.*, “Study of prompt D^0 meson production in $p\text{Pb}$ collisions at $\sqrt{s_{NN}} = 5$ TeV”, *JHEP* **10** (2017) 090, [arXiv:1707.02750](https://arxiv.org/abs/1707.02750) [hep-ex].
- [87] **ALICE** Collaboration, S. Acharya *et al.*, “Charm-quark fragmentation fractions and production cross section at midrapidity in pp collisions at the LHC”, *Phys. Rev. D* **105** (2022) L011103, [arXiv:2105.06335](https://arxiv.org/abs/2105.06335) [nucl-ex].
- [88] K. J. Eskola, H. Paukkunen, and C. A. Salgado, “EPS09: A New Generation of NLO and LO Nuclear Parton Distribution Functions”, *JHEP* **04** (2009) 065, [arXiv:0902.4154](https://arxiv.org/abs/0902.4154) [hep-ph].
- [89] S. Aronson, E. Borras, B. Odegaard, R. Sharma, and I. Vitev, “Collisional and thermal dissociation of J/ψ and Υ states at the LHC”, *Phys. Lett. B* **778** (2018) 384–391, [arXiv:1709.02372](https://arxiv.org/abs/1709.02372) [hep-ph].
- [90] Y. Makris and I. Vitev, “An Effective Theory of Quarkonia in QCD Matter”, *JHEP* **10** (2019) 111, [arXiv:1906.04186](https://arxiv.org/abs/1906.04186) [hep-ph].

- [91] G. T. Bodwin, E. Braaten, and G. P. Lepage, “Rigorous QCD analysis of inclusive annihilation and production of heavy quarkonium”, *Phys. Rev. D* **51** (1995) 1125–1171, arXiv:hep-ph/9407339. [Erratum: Phys.Rev.D 55, 5853 (1997)].
- [92] M. Yang, S. Zheng, B. Tong, J. Zhao, W. Ouyang, K. Zhou, and B. Chen, “Bottom energy loss and non-prompt J/ ψ production in relativistic heavy ion collisions”, *Phys. Rev. C* **107** (2023) 054917, arXiv:2302.06179 [nucl-th].
- [93] A. Beraudo, A. De Pace, M. Monteno, M. Nardi, and F. Prino, “Rapidity dependence of heavy-flavour production in heavy-ion collisions within a full 3+1 transport approach: quenching, elliptic and directed flow”, *JHEP* **05** (2021) 279, arXiv:2102.08064 [hep-ph].
- [94] A. Beraudo, A. De Pace, M. Monteno, M. Nardi, and F. Prino, “Heavy flavors in heavy-ion collisions: quenching, flow and correlations”, *Eur. Phys. J. C* **75** (2015) 121, arXiv:1410.6082 [hep-ph].
- [95] S. Shi, J. Liao, and M. Gyulassy, “Global constraints from RHIC and LHC on transport properties of QCD fluids in CUJET/CIBJET framework”, *Chin. Phys. C* **43** (2019) 044101, arXiv:1808.05461 [hep-ph].
- [96] S. Shi, J. Liao, and M. Gyulassy, “Probing the Color Structure of the Perfect QCD Fluids via Soft-Hard-Event-by-Event Azimuthal Correlations”, *Chin. Phys. C* **42** (2018) 104104, arXiv:1804.01915 [hep-ph].
- [97] M. Nahrgang, J. Aichelin, P. B. Gossiaux, and K. Werner, “Toward a consistent evolution of the quark-gluon plasma and heavy quarks”, *Phys. Rev. C* **93** (2016) 044909, arXiv:1602.03544 [nucl-th].
- [98] M. Cacciari, P. Nason, and R. Vogt, “QCD predictions for charm and bottom production at RHIC”, *Phys. Rev. Lett.* **95** (2005) 122001, arXiv:hep-ph/0502203.
- [99] S. Frixione, P. Nason, and G. Ridolfi, “A Positive-weight next-to-leading-order Monte Carlo for heavy flavour hadroproduction”, *JHEP* **09** (2007) 126, arXiv:0707.3088 [hep-ph].
- [100] J. Pumplin, D. R. Stump, J. Huston, H. L. Lai, P. M. Nadolsky, and W. K. Tung, “New generation of parton distributions with uncertainties from global QCD analysis”, *JHEP* **07** (2002) 012, arXiv:hep-ph/0201195.
- [101] C. Peterson, D. Schlatter, I. Schmitt, and P. M. Zerwas, “Scaling violations in inclusive e^+e^- annihilation spectra”, *Phys. Rev. D* **27** (Jan, 1983) 105–111.
- [102] P. B. Gossiaux and J. Aichelin, “Towards an understanding of the RHIC single electron data”, *Phys. Rev. C* **78** (2008) 014904, arXiv:0802.2525 [hep-ph].
- [103] K. Werner, I. Karpenko, T. Pierog, M. Bleicher, and K. Mikhailov, “Event-by-event simulation of the three-dimensional hydrodynamic evolution from flux tube initial conditions in ultrarelativistic heavy ion collisions”, *Phys. Rev. C* **82** (Oct, 2010) 044904.
<https://link.aps.org/doi/10.1103/PhysRevC.82.044904>.
- [104] K. Werner, I. Karpenko, M. Bleicher, T. Pierog, and S. Porteboeuf-Houssais, “Jets, bulk matter, and their interaction in heavy ion collisions at several tev”, *Phys. Rev. C* **85** (Jun, 2012) 064907.
<https://link.aps.org/doi/10.1103/PhysRevC.85.064907>.
- [105] S.-Q. Li, W.-J. Xing, X.-Y. Wu, S. Cao, and G.-Y. Qin, “Scaling behaviors of heavy flavor meson suppression and flow in different nuclear collision systems at the LHC”, *Eur. Phys. J. C* **81** (2021) 1035, arXiv:2108.06648 [hep-ph].

- [106] W.-J. Xing, G.-Y. Qin, and S. Cao, “Perturbative and non-perturbative interactions between heavy quarks and quark-gluon plasma within a unified approach”, *Phys. Lett. B* **838** (2023) 137733, arXiv:2112.15062 [hep-ph].
- [107] D. Zivic, I. Salom, J. Auvinen, P. Huovinen, and M. Djordjevic, “DREENA-A framework as a QGP tomography tool”, *Front. in Phys.* **10** (2022) 957019, arXiv:2110.01544 [nucl-th].
- [108] S. Stojku, J. Auvinen, M. Djordjevic, P. Huovinen, and M. Djordjevic, “Early evolution constrained by high- p_T quark-gluon plasma tomography”, *Phys. Rev. C* **105** (2022) L021901, arXiv:2008.08987 [nucl-th].
- [109] S. Dulat, T.-J. Hou, J. Gao, M. Guzzi, J. Huston, P. Nadolsky, J. Pumplin, C. Schmidt, D. Stump, and C. P. Yuan, “New parton distribution functions from a global analysis of quantum chromodynamics”, *Phys. Rev. D* **93** (2016) 033006, arXiv:1506.07443 [hep-ph].
- [110] K. J. Eskola, P. Paakkinen, H. Paukkunen, and C. A. Salgado, “EPPS16: Nuclear parton distributions with LHC data”, *Eur. Phys. J. C* **77** (2017) 163, arXiv:1612.05741 [hep-ph].
- [111] S. Cao, K.-J. Sun, S.-Q. Li, S. Y. F. Liu, W.-J. Xing, G.-Y. Qin, and C. M. Ko, “Charmed hadron chemistry in relativistic heavy-ion collisions”, *Phys. Lett. B* **807** (2020) 135561, arXiv:1911.00456 [nucl-th].
- [112] R. Sharma, I. Vitev, and B.-W. Zhang, “Light-cone wave function approach to open heavy flavor dynamics in QCD matter”, *Phys. Rev. C* **80** (Nov, 2009) 054902.
- [113] V. G. Kartvelishvili, A. K. Likhoded, and V. A. Petrov, “On the Fragmentation Functions of Heavy Quarks Into Hadrons”, *Phys. Lett. B* **78** (1978) 615–617.
- [114] ALICE Collaboration, “ALICE upgrades during the LHC Long Shutdown 2”, arXiv:2302.01238 [physics.ins-det].

A The ALICE Collaboration

- S. Acharya ¹²⁸, D. Adamová ⁸⁷, G. Aglieri Rinella ³³, M. Agnello ³⁰, N. Agrawal ⁵², Z. Ahammed ¹³⁶, S. Ahmad ¹⁶, S.U. Ahn ⁷², I. Ahuja ³⁸, A. Akindinov ¹⁴², M. Al-Turany ⁹⁸, D. Aleksandrov ¹⁴², B. Alessandro ⁵⁷, H.M. Alfanda ⁶, R. Alfaro Molina ⁶⁸, B. Ali ¹⁶, A. Alici ²⁶, N. Alizadehvandchali ¹¹⁷, A. Alkin ³³, J. Alme ²¹, G. Alocco ⁵³, T. Alt ⁶⁵, A.R. Altamura ⁵¹, I. Altsybeev ⁹⁶, J.R. Alvarado ⁴⁵, M.N. Anaam ⁶, C. Andrei ⁴⁶, N. Andreou ¹¹⁶, A. Andronic ¹²⁷, V. Anguelov ⁹⁵, F. Antinori ⁵², P. Antonioli ⁵², N. Apadula ⁷⁵, L. Aphecetche ¹⁰⁴, H. Appelshäuser ⁶⁵, C. Arata ⁷⁴, S. Arcelli ²⁶, M. Aresti ²³, R. Arnaldi ⁵⁷, J.G.M.C.A. Arneiro ¹¹¹, I.C. Arsene ²⁰, M. Arslanbek ¹³⁹, A. Augustinus ³³, R. Averbeck ⁹⁸, M.D. Azmi ¹⁶, H. Baba ¹²⁵, A. Badalà ⁵⁴, J. Bae ¹⁰⁵, Y.W. Baek ⁴¹, X. Bai ¹²¹, R. Bailhache ⁶⁵, Y. Bailung ⁴⁹, A. Balbino ³⁰, A. Baldissari ¹³¹, B. Balis ², D. Banerjee ⁴, Z. Banoo ⁹², R. Barbera ²⁷, F. Barile ³², L. Barioglio ⁹⁶, M. Barlou ⁷⁹, B. Barman ⁴², G.G. Barnaföldi ⁴⁷, L.S. Barnby ⁸⁶, V. Barret ¹²⁸, L. Barreto ¹¹¹, C. Bartels ¹²⁰, K. Barth ³³, E. Bartsch ⁶⁵, N. Bastid ¹²⁸, S. Basu ⁷⁶, G. Batigne ¹⁰⁴, D. Battistini ⁹⁶, B. Batyunya ¹⁴³, D. Bauri ⁴⁸, J.L. Bazo Alba ¹⁰², I.G. Bearden ⁸⁴, C. Beattie ¹³⁹, P. Becht ⁹⁸, D. Behera ⁴⁹, I. Belikov ¹³⁰, A.D.C. Bell Hechavarria ¹²⁷, F. Bellini ²⁶, R. Bellwied ¹¹⁷, S. Belokurova ¹⁴², Y.A.V. Beltran ⁴⁵, G. Bencedi ⁴⁷, S. Beole ²⁵, Y. Berdnikov ¹⁴², A. Berdnikova ⁹⁵, L. Bergmann ⁹⁵, M.G. Besoiu ⁶⁴, L. Betev ³³, P.P. Bhaduri ¹³⁶, A. Bhasin ⁹², M.A. Bhat ⁴, B. Bhattacharjee ⁴², L. Bianchi ²⁵, N. Bianchi ⁵⁰, J. Bielčík ³⁶, J. Bielčíková ⁸⁷, J. Biernat ¹⁰⁸, A.P. Bigot ¹³⁰, A. Bilandzic ⁹⁶, G. Biro ⁴⁷, S. Biswas ⁴, N. Bize ¹⁰⁴, J.T. Blair ¹⁰⁹, D. Blau ¹⁴², M.B. Blidaru ⁹⁸, N. Bluhme ³⁹, C. Blume ⁶⁵, G. Boca ^{22,56}, F. Bock ⁸⁸, T. Bodova ²¹, A. Bogdanov ¹⁴², S. Boi ²³, J. Bok ⁵⁹, L. Boldizsár ⁴⁷, M. Bombara ³⁸, P.M. Bond ³³, G. Bonomi ^{135,56}, H. Borel ¹³¹, A. Borissov ¹⁴², A.G. Borquez Carcamo ⁹⁵, H. Bossi ¹³⁹, E. Botta ²⁵, Y.E.M. Bouziani ⁶⁵, L. Bratrud ⁶⁵, P. Braun-Munzinger ⁹⁸, M. Bregant ¹¹¹, M. Broz ³⁶, G.E. Bruno ^{97,32}, M.D. Buckland ²⁴, D. Budnikov ¹⁴², H. Buesching ⁶⁵, S. Bufalino ³⁰, P. Buhler ¹⁰³, N. Burmasov ¹⁴², Z. Buthelezi ^{69,124}, A. Bylinkin ²¹, S.A. Bysiak ¹⁰⁸, M. Cai ⁶, H. Caines ¹³⁹, A. Caliva ²⁹, E. Calvo Villar ¹⁰², J.M.M. Camacho ¹¹⁰, P. Camerini ²⁴, F.D.M. Canedo ¹¹¹, S.L. Cantway ¹³⁹, M. Carabas ¹¹⁴, A.A. Carballo ³³, F. Carnesecchi ³³, R. Caron ¹²⁹, L.A.D. Carvalho ¹¹¹, J. Castillo Castellanos ¹³¹, F. Catalano ^{33,25}, C. Ceballos Sanchez ¹⁴³, I. Chakaberia ⁷⁵, P. Chakraborty ⁴⁸, S. Chandra ¹³⁶, S. Chapeland ³³, M. Chartier ¹²⁰, S. Chattopadhyay ¹³⁶, S. Chattopadhyay ¹⁰⁰, T. Cheng ^{98,6}, C. Cheshkov ¹²⁹, B. Cheynis ¹²⁹, V. Chibante Barroso ³³, D.D. Chinellato ¹¹², E.S. Chizzali ^{II,96}, J. Cho ⁵⁹, S. Cho ⁵⁹, P. Chochula ³³, D. Choudhury ⁴², P. Christakoglou ⁸⁵, C.H. Christensen ⁸⁴, P. Christiansen ⁷⁶, T. Chujo ¹²⁶, M. Ciacco ³⁰, C. Cicalo ⁵³, F. Cindolo ⁵², M.R. Ciupek ⁹⁸, G. Clai III,52, F. Colamaria ⁵¹, J.S. Colburn ¹⁰¹, D. Colella ^{97,32}, M. Colocci ²⁶, M. Concias ^{IV,33}, G. Conesa Balbastre ⁷⁴, Z. Conesa del Valle ¹³², G. Contin ²⁴, J.G. Contreras ³⁶, M.L. Coquet ¹³¹, P. Cortese ^{134,57}, M.R. Cosentino ¹¹³, F. Costa ³³, S. Costanza ^{22,56}, C. Cot ¹³², J. Crkovská ⁹⁵, P. Crochet ¹²⁸, R. Cruz-Torres ⁷⁵, P. Cui ⁶, A. Dainese ⁵⁵, M.C. Danisch ⁹⁵, A. Danu ⁶⁴, P. Das ⁸¹, P. Das ⁴, S. Das ⁴, A.R. Dash ¹²⁷, S. Dash ⁴⁸, A. De Caro ²⁹, G. de Cataldo ⁵¹, J. de Cuveland ³⁹, A. De Falco ²³, D. De Gruttola ²⁹, N. De Marco ⁵⁷, C. De Martin ²⁴, S. De Pasquale ²⁹, R. Deb ¹³⁵, R. Del Grande ⁹⁶, L. Dello Stritto ²⁹, W. Deng ⁶, P. Dhankher ¹⁹, D. Di Bari ³², A. Di Mauro ³³, B. Diab ¹³¹, R.A. Diaz ^{143,7}, T. Dietel ¹¹⁵, Y. Ding ⁶, J. Ditzel ⁶⁵, R. Divià ³³, D.U. Dixit ¹⁹, Ø. Djupsland ²¹, U. Dmitrieva ¹⁴², A. Dobrin ⁶⁴, B. Dönigus ⁶⁵, J.M. Dubinski ¹³⁷, A. Dubla ⁹⁸, S. Dudi ⁹¹, P. Dupieux ¹²⁸, M. Durkac ¹⁰⁷, N. Dzalaiova ¹³, T.M. Eder ¹²⁷, R.J. Ehlers ⁷⁵, F. Eisenhut ⁶⁵, R. Ejima ⁹³, D. Elia ⁵¹, B. Erazmus ¹⁰⁴, F. Ercolelli ²⁶, B. Espagnon ¹³², G. Eulisse ³³, D. Evans ¹⁰¹, S. Evdokimov ¹⁴², L. Fabbietti ⁹⁶, M. Faggion ²⁸, J. Faivre ⁷⁴, F. Fan ⁶, W. Fan ⁷⁵, A. Fantoni ⁵⁰, M. Fasel ⁸⁸, A. Feliciello ⁵⁷, G. Feofilov ¹⁴², A. Fernández Téllez ⁴⁵, L. Ferrandi ¹¹¹, M.B. Ferrer ³³, A. Ferrero ¹³¹, C. Ferrero ⁵⁷, A. Ferretti ²⁵, V.J.G. Feuillard ⁹⁵, V. Filova ³⁶, D. Finogeev ¹⁴², F.M. Fionda ⁵³, E. Flatland ³³, F. Flor ¹¹⁷, A.N. Flores ¹⁰⁹, S. Foertsch ⁶⁹, I. Fokin ⁹⁵, S. Fokin ¹⁴², E. Fragiocomo ⁵⁸, E. Frajna ⁴⁷, U. Fuchs ³³, N. Funicello ²⁹, C. Furget ⁷⁴, A. Furs ¹⁴², T. Fusayasu ⁹⁹, J.J. Gaardhøje ⁸⁴, M. Gagliardi ²⁵, A.M. Gago ¹⁰², T. Gahlaud ⁴⁸, C.D. Galvan ¹¹⁰, D.R. Gangadharan ¹¹⁷, P. Ganoti ⁷⁹, C. Garabatos ⁹⁸, T. García Chávez ⁴⁵, E. Garcia-Solis ⁹, C. Gargiulo ³³, P. Gasik ⁹⁸, A. Gautam ¹¹⁹, M.B. Gay Ducati ⁶⁷, M. Germain ¹⁰⁴, A. Ghimouz ¹²⁶, C. Ghosh ¹³⁶, M. Giacalone ⁵², G. Gioachin ³⁰, P. Giubellino ^{98,57}, P. Giubilato ²⁸, A.M.C. Glaenzer ¹³¹, P. Glässel ⁹⁵, E. Glimos ¹²³, D.J.Q. Goh ⁷⁷, V. Gonzalez ¹³⁸, P. Gordeev ¹⁴², M. Gorgon ², K. Goswami ⁴⁹, S. Gotovac ³⁴, V. Grabski ⁶⁸, L.K. Graczykowski ¹³⁷, E. Grecka ⁸⁷, A. Grelli ⁶⁰, C. Grigoras ³³, V. Grigoriev ¹⁴², S. Grigoryan ^{143,1}, F. Grossa ³³, J.F. Grosse-Oetringhaus ³³, R. Grossi ⁹⁸, D. Grund ³⁶, N.A. Grunwald ⁹⁵, G.G. Guardiano ¹¹², R. Guernane ⁷⁴, M. Guilbaud ¹⁰⁴,

- K. Gulbrandsen⁸⁴, T. Gündem⁶⁵, T. Gunji¹²⁵, W. Guo⁶, A. Gupta⁹², R. Gupta⁹², R. Gupta⁴⁹, K. Gwizdziel¹³⁷, L. Gyulai⁴⁷, C. Hadjidakis¹³², F.U. Haider⁹², S. Haidlova³⁶, H. Hamagaki⁷⁷, A. Hamdi⁷⁵, Y. Han¹⁴⁰, B.G. Hanley¹³⁸, R. Hannigan¹⁰⁹, J. Hansen⁷⁶, M.R. Haque¹³⁷, J.W. Harris¹³⁹, A. Harton⁹, H. Hassan¹¹⁸, D. Hatzifotiadou⁵², P. Hauer⁴³, L.B. Havener¹³⁹, S.T. Heckel⁹⁶, E. Hellbär⁹⁸, H. Helstrup³⁵, M. Hemmer⁶⁵, T. Herman³⁶, G. Herrera Corral⁸, F. Herrmann¹²⁷, S. Herrmann¹²⁹, K.F. Hetland³⁵, B. Heybeck⁶⁵, H. Hillemanns³³, B. Hippolyte¹³⁰, F.W. Hoffmann⁷¹, B. Hofman⁶⁰, G.H. Hong¹⁴⁰, M. Horst⁹⁶, A. Horzyk², Y. Hou⁶, P. Hristov³³, C. Hughes¹²³, P. Huhn⁶⁵, L.M. Huhta¹¹⁸, T.J. Humanic⁸⁹, A. Hutson¹¹⁷, D. Hutter³⁹, R. Ilkaev¹⁴², H. Ilyas¹⁴, M. Inaba¹²⁶, G.M. Innocenti³³, M. Ippolitov¹⁴², A. Isakov^{85,87}, T. Isidori¹¹⁹, M.S. Islam¹⁰⁰, M. Ivanov¹³, M. Ivanov⁹⁸, V. Ivanov¹⁴², K.E. Iversen⁷⁶, M. Jablonski², B. Jacak⁷⁵, N. Jacazio²⁶, P.M. Jacobs⁷⁵, S. Jadlovska¹⁰⁷, J. Jadlovsky¹⁰⁷, S. Jaelani⁸³, C. Jahnke¹¹¹, M.J. Jakubowska¹³⁷, M.A. Janik¹³⁷, T. Janson⁷¹, S. Ji¹⁷, S. Jia¹⁰, A.A.P. Jimenez⁶⁶, F. Jonas^{88,127}, D.M. Jones¹²⁰, J.M. Jowett^{33,98}, J. Jung⁶⁵, M. Jung⁶⁵, A. Junique³³, A. Jusko¹⁰¹, M.J. Kabus^{33,137}, J. Kaewjai¹⁰⁶, P. Kalinak⁶¹, A.S. Kalteyer⁹⁸, A. Kalweit³³, V. Kaplin¹⁴², A. Karasu Uysal⁷³, D. Karatovic⁹⁰, O. Karavichev¹⁴², T. Karavicheva¹⁴², P. Karczmarczyk¹³⁷, E. Karpechev¹⁴², U. Kebschull⁷¹, R. Keidel¹⁴¹, D.L.D. Keijdener⁶⁰, M. Keil³³, B. Ketzer⁴³, S.S. Khade⁴⁹, A.M. Khan¹²¹, S. Khan¹⁶, A. Khanzadeev¹⁴², Y. Kharlov¹⁴², A. Khatun¹¹⁹, A. Khuntia³⁶, B. Kileng³⁵, B. Kim¹⁰⁵, C. Kim¹⁷, D.J. Kim¹¹⁸, E.J. Kim⁷⁰, J. Kim¹⁴⁰, J.S. Kim⁴¹, J. Kim⁵⁹, J. Kim⁷⁰, M. Kim¹⁹, S. Kim¹⁸, T. Kim¹⁴⁰, K. Kimura⁹³, S. Kirsch⁶⁵, I. Kisel³⁹, S. Kiselev¹⁴², A. Kisiel¹³⁷, J.P. Kitowski², J.L. Klay⁵, J. Klein³³, S. Klein⁷⁵, C. Klein-Bösing¹²⁷, M. Kleiner⁶⁵, T. Klemenz⁹⁶, A. Kluge³³, A.G. Knospe¹¹⁷, C. Kobdaj¹⁰⁶, T. Kollegger⁹⁸, A. Kondratyev¹⁴³, N. Kondratyeva¹⁴², E. Kondratyuk¹⁴², J. Konig⁶⁵, S.A. Konigstorfer⁹⁶, P.J. Konopka³³, G. Kornakov¹³⁷, M. Korwieser⁹⁶, S.D. Koryciak², A. Kotliarov⁸⁷, V. Kovalenko¹⁴², M. Kowalski¹⁰⁸, V. Kozhuharov³⁷, I. Králik⁶¹, A. Kravčáková³⁸, L. Krcal^{33,39}, M. Krivda^{101,61}, F. Krizek⁸⁷, K. Krizkova Gajdosova³³, M. Kroesen⁹⁵, M. Krüger⁶⁵, D.M. Krupova³⁶, E. Kryshen¹⁴², V. Kućera⁵⁹, C. Kuhn¹³⁰, P.G. Kuijer⁸⁵, T. Kumaoka¹²⁶, D. Kumar¹³⁶, L. Kumar⁹¹, N. Kumar⁹¹, S. Kumar³², S. Kundu³³, P. Kurashvili⁸⁰, A. Kurepin¹⁴², A.B. Kurepin¹⁴², A. Kuryakin¹⁴², S. Kushpil⁸⁷, V. Kuskov¹⁴², M.J. Kweon⁵⁹, Y. Kwon¹⁴⁰, S.L. La Pointe³⁹, P. La Rocca²⁷, A. Lakrathok¹⁰⁶, M. Lamanna³³, A.R. Landou^{74,116}, R. Langoy¹²², P. Larionov³³, E. Laudi³³, L. Lautner^{33,96}, R. Lavicka¹⁰³, R. Lea^{135,56}, H. Lee¹⁰⁵, I. Legrand⁴⁶, G. Legras¹²⁷, J. Lehrbach³⁹, T.M. Lelek², R.C. Lemmon⁸⁶, I. León Monzón¹¹⁰, M.M. Lesch⁹⁶, E.D. Lesser¹⁹, P. Lévai⁴⁷, X. Li¹⁰, J. Lien¹²², R. Lietava¹⁰¹, I. Likmeta¹¹⁷, B. Lim²⁵, S.H. Lim¹⁷, V. Lindenstruth³⁹, A. Lindner⁴⁶, C. Lippmann⁹⁸, D.H. Liu⁶, J. Liu¹²⁰, G.S.S. Liveraro¹¹², I.M. Lofnes²¹, C. Loizides⁸⁸, S. Lokos¹⁰⁸, J. Lömkér⁶⁰, P. Loncar³⁴, X. Lopez¹²⁸, E. López Torres⁷, P. Lu^{98,121}, F.V. Lugo⁶⁸, J.R. Luhder¹²⁷, M. Lunardon²⁸, G. Luparello⁵⁸, Y.G. Ma⁴⁰, M. Mager³³, A. Maire¹³⁰, E.M. Majerz², M.V. Makariev³⁷, M. Malaev¹⁴², G. Malfattore²⁶, N.M. Malik⁹², Q.W. Malik²⁰, S.K. Malik⁹², L. Malinina^{I,VII,143}, D. Mallick^{132,81}, N. Mallick⁴⁹, G. Mandaglio^{31,54}, S.K. Mandal⁸⁰, V. Manko¹⁴², F. Manso¹²⁸, V. Manzari⁵¹, Y. Mao⁶, R.W. Marcjan², G.V. Margagliotti²⁴, A. Margotti⁵², A. Marín⁹⁸, C. Markert¹⁰⁹, P. Martinengo³³, M.I. Martínez⁴⁵, G. Martínez García¹⁰⁴, M.P.P. Martins¹¹¹, S. Masciocchi⁹⁸, M. Masera²⁵, A. Masoni⁵³, L. Massacrier¹³², O. Massen⁶⁰, A. Mastroserio^{133,51}, O. Matonoha⁷⁶, S. Mattiazzo²⁸, A. Matyja¹⁰⁸, C. Mayer¹⁰⁸, A.L. Mazuecos³³, F. Mazzaschi²⁵, M. Mazzilli³³, J.E. Mdhluli¹²⁴, Y. Melikyan⁴⁴, A. Menchaca-Rocha⁶⁸, J.E.M. Mendez⁶⁶, E. Meninno¹⁰³, A.S. Menon¹¹⁷, M. Meres¹³, S. Mhlanga^{115,69}, Y. Miake¹²⁶, L. Micheletti³³, D.L. Mihaylov⁹⁶, K. Mikhaylov^{143,142}, A.N. Mishra⁴⁷, D. Miśkowiec⁹⁸, A. Modak⁴, B. Mohanty⁸¹, M. Mohisin Khan^{V,16}, M.A. Molander⁴⁴, S. Monira¹³⁷, C. Mordasini¹¹⁸, D.A. Moreira De Godoy¹²⁷, I. Morozov¹⁴², A. Morsch³³, T. Mrnjavac³³, V. Muccifora⁵⁰, S. Muhuri¹³⁶, J.D. Mulligan⁷⁵, A. Mulliri²³, M.G. Munhoz¹¹¹, R.H. Munzer⁶⁵, H. Murakami¹²⁵, S. Murray¹¹⁵, L. Musa³³, J. Musinsky⁶¹, J.W. Myrcha¹³⁷, B. Naik¹²⁴, A.I. Nambrath¹⁹, B.K. Nandi⁴⁸, R. Nania⁵², E. Nappi⁵¹, A.F. Nassirpour¹⁸, A. Nath⁹⁵, C. Nattrass¹²³, M.N. Naydenov³⁷, A. Neagu²⁰, A. Negru¹¹⁴, E. Nekrasova¹⁴², L. Nellen⁶⁶, R. Nepeivoda⁷⁶, S. Nese²⁰, G. Neskovic³⁹, N. Nicassio⁵¹, B.S. Nielsen⁸⁴, E.G. Nielsen⁸⁴, S. Nikolaev¹⁴², S. Nikulin¹⁴², V. Nikulin¹⁴², F. Noferini⁵², S. Noh¹², P. Nomokonov¹⁴³, J. Norman¹²⁰, N. Novitzky⁸⁸, P. Nowakowski¹³⁷, A. Nyanin¹⁴², J. Nystrand²¹, M. Ogino⁷⁷, S. Oh¹⁸, A. Ohlson⁷⁶, V.A. Okorokov¹⁴², J. Oleniacz¹³⁷, A.C. Oliveira Da Silva¹²³, A. Onnerstad¹¹⁸, C. Oppedisano⁵⁷, A. Ortiz Velasquez⁶⁶, J. Otwinowski¹⁰⁸, M. Oya⁹³, K. Oyama⁷⁷, Y. Pachmayer⁹⁵, S. Padhan⁴⁸, D. Pagano^{135,56}, G. Paić⁶⁶, S. Paisano-Guzmán⁴⁵,

- A. Palasciano ⁵¹, S. Panebianco ¹³¹, H. Park ¹²⁶, H. Park ¹⁰⁵, J. Park ⁵⁹, J.E. Parkkila ³³, Y. Patley ⁴⁸, R.N. Patra ⁹², B. Paul ²³, H. Pei ⁶, T. Peitzmann ⁶⁰, X. Peng ¹¹, M. Pennisi ²⁵, S. Perciballi ²⁵, D. Peresunko ¹⁴², G.M. Perez ⁷, Y. Pestov ¹⁴², V. Petrov ¹⁴², M. Petrovici ⁴⁶, R.P. Pezzi ^{104,67}, S. Piano ⁵⁸, M. Pikna ¹³, P. Pillot ¹⁰⁴, O. Pinazza ^{52,33}, L. Pinsky ¹¹⁷, C. Pinto ⁹⁶, S. Pisano ⁵⁰, M. Płoskoń ⁷⁵, M. Planinic ⁹⁰, F. Pliquet ⁶⁵, M.G. Poghosyan ⁸⁸, B. Polichtchouk ¹⁴², S. Politano ³⁰, N. Poljak ⁹⁰, A. Pop ⁴⁶, S. Porteboeuf-Houssais ¹²⁸, V. Pozdniakov ¹⁴³, I.Y. Pozos ⁴⁵, K.K. Pradhan ⁴⁹, S.K. Prasad ⁴, S. Prasad ⁴⁹, R. Preghenella ⁵², F. Prino ⁵⁷, C.A. Pruneau ¹³⁸, I. Pshenichnov ¹⁴², M. Puccio ³³, S. Pucillo ²⁵, Z. Pugelova ¹⁰⁷, S. Qiu ⁸⁵, L. Quaglia ²⁵, S. Ragoni ¹⁵, A. Rai ¹³⁹, A. Rakotozafindrabe ¹³¹, L. Ramello ^{134,57}, F. Rami ¹³⁰, T.A. Rancien ⁷⁴, M. Rasa ²⁷, S.S. Räsänen ⁴⁴, R. Rath ⁵², M.P. Rauch ²¹, I. Ravasenga ⁸⁵, K.F. Read ^{88,123}, C. Reckziegel ¹¹³, A.R. Redelbach ³⁹, K. Redlich ^{VI,80}, C.A. Reetz ⁹⁸, H.D. Regules-Medel ⁴⁵, A. Rehman ²¹, F. Reidt ³³, H.A. Reme-Ness ³⁵, Z. Rescakova ³⁸, K. Reygers ⁹⁵, A. Riabov ¹⁴², V. Riabov ¹⁴², R. Ricci ²⁹, M. Richter ²⁰, A.A. Riedel ⁹⁶, W. Riegler ³³, A.G. Riffero ²⁵, C. Ristea ⁶⁴, M.V. Rodriguez ³³, M. Rodríguez Cahuantzi ⁴⁵, S.A. Rodríguez Ramírez ⁴⁵, K. Røed ²⁰, R. Rogalev ¹⁴², E. Rogochaya ¹⁴³, T.S. Rogoschinski ⁶⁵, D. Rohr ³³, D. Röhrich ²¹, P.F. Rojas ⁴⁵, S. Rojas Torres ³⁶, P.S. Rokita ¹³⁷, G. Romanenko ²⁶, F. Ronchetti ⁵⁰, A. Rosano ^{31,54}, E.D. Rosas ⁶⁶, K. Roslon ¹³⁷, A. Rossi ⁵⁵, A. Roy ⁴⁹, S. Roy ⁴⁸, N. Rubini ²⁶, D. Ruggiano ¹³⁷, R. Rui ²⁴, P.G. Russek ², R. Russo ⁸⁵, A. Rustamov ⁸², E. Ryabinkin ¹⁴², Y. Ryabov ¹⁴², A. Rybicki ¹⁰⁸, H. Rytkonen ¹¹⁸, J. Ryu ¹⁷, W. Rzesz ¹³⁷, O.A.M. Saarimaki ⁴⁴, S. Sadhu ³², S. Sadovsky ¹⁴², J. Saetre ²¹, K. Šafářík ³⁶, P. Saha ⁴², S.K. Saha ⁴, S. Saha ⁸¹, B. Sahoo ⁴⁸, B. Sahoo ⁴⁹, R. Sahoo ⁴⁹, S. Sahoo ⁶², D. Sahu ⁴⁹, P.K. Sahu ⁶², J. Saini ¹³⁶, K. Sajdakova ³⁸, S. Sakai ¹²⁶, M.P. Salvan ⁹⁸, S. Sambyal ⁹², D. Samitz ¹⁰³, I. Sanna ^{33,96}, T.B. Saramela ¹¹¹, P. Sarma ⁴², V. Sarritzu ²³, V.M. Sarti ⁹⁶, M.H.P. Sas ³³, S. Sawan ⁸¹, J. Schambach ⁸⁸, H.S. Scheid ⁶⁵, C. Schiaua ⁴⁶, R. Schicker ⁹⁵, F. Schlepper ⁹⁵, A. Schmeh ⁹⁸, C. Schmidt ⁹⁸, H.R. Schmidt ⁹⁴, M.O. Schmidt ³³, M. Schmidt ⁹⁴, N.V. Schmidt ⁸⁸, A.R. Schmier ¹²³, R. Schotter ¹³⁰, A. Schröter ³⁹, J. Schukraft ³³, K. Schweda ⁹⁸, G. Scioli ²⁶, E. Scomparin ⁵⁷, J.E. Seger ¹⁵, Y. Sekiguchi ¹²⁵, D. Sekihata ¹²⁵, M. Selina ⁸⁵, I. Selyuzhenkov ⁹⁸, S. Senyukov ¹³⁰, J.J. Seo ^{95,59}, D. Serebryakov ¹⁴², L. Šerkšnytė ⁹⁶, A. Sevcenco ⁶⁴, T.J. Shaba ⁶⁹, A. Shabetai ¹⁰⁴, R. Shahoyan ³³, A. Shangaraev ¹⁴², A. Sharma ⁹¹, B. Sharma ⁹², D. Sharma ⁴⁸, H. Sharma ⁵⁵, M. Sharma ⁹², S. Sharma ⁷⁷, S. Sharma ⁹², U. Sharma ⁹², A. Shatat ¹³², O. Sheibani ¹¹⁷, K. Shigaki ⁹³, M. Shimomura ⁷⁸, J. Shin ¹², S. Shirinkin ¹⁴², Q. Shou ⁴⁰, Y. Sibiriak ¹⁴², S. Siddhanta ⁵³, T. Siemarczuk ⁸⁰, T.F. Silva ¹¹¹, D. Silvermyr ⁷⁶, T. Simantathammakul ¹⁰⁶, R. Simeonov ³⁷, B. Singh ⁹², B. Singh ⁹⁶, K. Singh ⁴⁹, R. Singh ⁸¹, R. Singh ⁹², R. Singh ⁴⁹, S. Singh ¹⁶, V.K. Singh ¹³⁶, V. Singhal ¹³⁶, T. Sinha ¹⁰⁰, B. Sitar ¹³, M. Sitta ^{134,57}, T.B. Skaali ²⁰, G. Skorodumovs ⁹⁵, M. Slupecki ⁴⁴, N. Smirnov ¹³⁹, R.J.M. Snellings ⁶⁰, E.H. Solheim ²⁰, J. Song ¹⁷, C. Sonnabend ^{33,98}, F. Soramel ²⁸, A.B. Soto-hernandez ⁸⁹, R. Spijkers ⁸⁵, I. Sputowska ¹⁰⁸, J. Staa ⁷⁶, J. Stachel ⁹⁵, I. Stan ⁶⁴, P.J. Steffanic ¹²³, S.F. Stiefelmaier ⁹⁵, D. Stocco ¹⁰⁴, I. Storehaug ²⁰, P. Stratmann ¹²⁷, S. Strazzi ²⁶, A. Sturniolo ^{31,54}, C.P. Stylianidis ⁸⁵, A.A.P. Suwaide ¹¹¹, C. Suire ¹³², M. Sukhanov ¹⁴², M. Suljic ³³, R. Sultanov ¹⁴², V. Sumberia ⁹², S. Sumowidago ⁸³, S. Swain ⁶², I. Szarka ¹³, M. Szymkowski ¹³⁷, S.F. Taghavi ⁹⁶, G. Taillepied ⁹⁸, J. Takahashi ¹¹², G.J. Tambave ⁸¹, S. Tang ⁶, Z. Tang ¹²¹, J.D. Tapia Takaki ¹¹⁹, N. Tapus ¹¹⁴, L.A. Tarasovicova ¹²⁷, M.G. Tarzila ⁴⁶, G.F. Tassielli ³², A. Tauro ³³, A. Tavira García ¹³², G. Tejeda Muñoz ⁴⁵, A. Telesca ³³, L. Terlizzi ²⁵, C. Terrevoli ¹¹⁷, S. Thakur ⁴, D. Thomas ¹⁰⁹, A. Tikhonov ¹⁴², N. Tiltmann ¹²⁷, A.R. Timmins ¹¹⁷, M. Tkacik ¹⁰⁷, T. Tkacik ¹⁰⁷, A. Toia ⁶⁵, R. Tokumoto ⁹³, K. Tomohiro ⁹³, N. Topilskaya ¹⁴², M. Toppi ⁵⁰, T. Tork ¹³², V.V. Torres ¹⁰⁴, A.G. Torres Ramos ³², A. Trifiró ^{31,54}, A.S. Triolo ^{33,31,54}, S. Tripathy ⁵², T. Tripathy ⁴⁸, S. Trogolo ³³, V. Trubnikov ³, W.H. Trzaska ¹¹⁸, T.P. Trzciński ¹³⁷, A. Tumkin ¹⁴², R. Turrisi ⁵⁵, T.S. Tveter ²⁰, K. Ullaland ²¹, B. Ulukutlu ⁹⁶, A. Uras ¹²⁹, G.L. Usai ²³, M. Vala ³⁸, N. Valle ²², L.V.R. van Doremalen ⁶⁰, M. van Leeuwen ⁸⁵, C.A. van Veen ⁹⁵, R.J.G. van Weelden ⁸⁵, P. Vande Vyvre ³³, D. Varga ⁴⁷, Z. Varga ⁴⁷, P. Vargas Torres ⁶⁶, M. Vasileiou ⁷⁹, A. Vasiliev ¹⁴², O. Vázquez Doce ⁵⁰, O. Vazquez Rueda ¹¹⁷, V. Vechernin ¹⁴², E. Vercellin ²⁵, S. Vergara Limón ⁴⁵, R. Verma ⁴⁸, L. Vermunt ⁹⁸, R. Vértesi ⁴⁷, M. Verweij ⁶⁰, L. Vickovic ³⁴, Z. Vilakazi ¹²⁴, O. Villalobos Baillie ¹⁰¹, A. Villani ²⁴, A. Vinogradov ¹⁴², T. Virgili ²⁹, M.M.O. Virta ¹¹⁸, V. Vislavicius ⁷⁶, A. Vodopyanov ¹⁴³, B. Volkel ³³, M.A. Völkl ⁹⁵, K. Voloshin ¹⁴², S.A. Voloshin ¹³⁸, G. Volpe ³², B. von Haller ³³, I. Vorobyev ⁹⁶, N. Vozniuk ¹⁴², J. Vrláková ³⁸, J. Wan ⁴⁰, C. Wang ⁴⁰, D. Wang ⁴⁰, Y. Wang ⁴⁰, Y. Wang ⁶, A. Wegrynek ³³, F.T. Weiglhofer ³⁹, S.C. Wenzel ³³, J.P. Wessels ¹²⁷, J. Wiechula ⁶⁵, J. Wikne ²⁰, G. Wilk ⁸⁰, J. Wilkinson ⁹⁸, G.A. Willems ¹²⁷, B. Windelband ⁹⁵, M. Winn ¹³¹, J.R. Wright ¹⁰⁹, W. Wu ⁴⁰, Y. Wu ¹²¹, R. Xu ⁶, A. Yadav ⁴³, A.K. Yadav ¹³⁶,

S. Yalcin ⁷³, Y. Yamaguchi ⁹³, S. Yang²¹, S. Yano ⁹³, Z. Yin ⁶, I.-K. Yoo ¹⁷, J.H. Yoon ⁵⁹, H. Yu¹²,
 S. Yuan²¹, A. Yuncu ⁹⁵, V. Zaccolo ²⁴, C. Zampolli ³³, F. Zanone ⁹⁵, N. Zardoshti ³³,
 A. Zarochentsev ¹⁴², P. Závada ⁶³, N. Zaviyalov¹⁴², M. Zhalov ¹⁴², B. Zhang ⁶, C. Zhang ¹³¹,
 L. Zhang ⁴⁰, S. Zhang ⁴⁰, X. Zhang ⁶, Y. Zhang¹²¹, Z. Zhang ⁶, M. Zhao ¹⁰, V. Zherebchevskii ¹⁴²,
 Y. Zhi¹⁰, D. Zhou ⁶, Y. Zhou ⁸⁴, J. Zhu ^{55,6}, Y. Zhu⁶, S.C. Zugravel ⁵⁷, N. Zurlo ^{135,56}

Affiliation Notes

^I Deceased

^{II} Also at: Max-Planck-Institut fur Physik, Munich, Germany

^{III} Also at: Italian National Agency for New Technologies, Energy and Sustainable Economic Development (ENEA), Bologna, Italy

^{IV} Also at: Dipartimento DET del Politecnico di Torino, Turin, Italy

^V Also at: Department of Applied Physics, Aligarh Muslim University, Aligarh, India

^{VI} Also at: Institute of Theoretical Physics, University of Wroclaw, Poland

^{VII} Also at: An institution covered by a cooperation agreement with CERN

Collaboration Institutes

¹ A.I. Alikhanyan National Science Laboratory (Yerevan Physics Institute) Foundation, Yerevan, Armenia

² AGH University of Krakow, Cracow, Poland

³ Bogolyubov Institute for Theoretical Physics, National Academy of Sciences of Ukraine, Kiev, Ukraine

⁴ Bose Institute, Department of Physics and Centre for Astroparticle Physics and Space Science (CAPSS), Kolkata, India

⁵ California Polytechnic State University, San Luis Obispo, California, United States

⁶ Central China Normal University, Wuhan, China

⁷ Centro de Aplicaciones Tecnológicas y Desarrollo Nuclear (CEADEN), Havana, Cuba

⁸ Centro de Investigación y de Estudios Avanzados (CINVESTAV), Mexico City and Mérida, Mexico

⁹ Chicago State University, Chicago, Illinois, United States

¹⁰ China Institute of Atomic Energy, Beijing, China

¹¹ China University of Geosciences, Wuhan, China

¹² Chungbuk National University, Cheongju, Republic of Korea

¹³ Comenius University Bratislava, Faculty of Mathematics, Physics and Informatics, Bratislava, Slovak Republic

¹⁴ COMSATS University Islamabad, Islamabad, Pakistan

¹⁵ Creighton University, Omaha, Nebraska, United States

¹⁶ Department of Physics, Aligarh Muslim University, Aligarh, India

¹⁷ Department of Physics, Pusan National University, Pusan, Republic of Korea

¹⁸ Department of Physics, Sejong University, Seoul, Republic of Korea

¹⁹ Department of Physics, University of California, Berkeley, California, United States

²⁰ Department of Physics, University of Oslo, Oslo, Norway

²¹ Department of Physics and Technology, University of Bergen, Bergen, Norway

²² Dipartimento di Fisica, Università di Pavia, Pavia, Italy

²³ Dipartimento di Fisica dell’Università and Sezione INFN, Cagliari, Italy

²⁴ Dipartimento di Fisica dell’Università and Sezione INFN, Trieste, Italy

²⁵ Dipartimento di Fisica dell’Università and Sezione INFN, Turin, Italy

²⁶ Dipartimento di Fisica e Astronomia dell’Università and Sezione INFN, Bologna, Italy

²⁷ Dipartimento di Fisica e Astronomia dell’Università and Sezione INFN, Catania, Italy

²⁸ Dipartimento di Fisica e Astronomia dell’Università and Sezione INFN, Padova, Italy

²⁹ Dipartimento di Fisica ‘E.R. Caianiello’ dell’Università and Gruppo Collegato INFN, Salerno, Italy

³⁰ Dipartimento DISAT del Politecnico and Sezione INFN, Turin, Italy

³¹ Dipartimento di Scienze MIFT, Università di Messina, Messina, Italy

³² Dipartimento Interateneo di Fisica ‘M. Merlin’ and Sezione INFN, Bari, Italy

³³ European Organization for Nuclear Research (CERN), Geneva, Switzerland

³⁴ Faculty of Electrical Engineering, Mechanical Engineering and Naval Architecture, University of Split, Split, Croatia

³⁵ Faculty of Engineering and Science, Western Norway University of Applied Sciences, Bergen, Norway

- ³⁶ Faculty of Nuclear Sciences and Physical Engineering, Czech Technical University in Prague, Prague, Czech Republic
³⁷ Faculty of Physics, Sofia University, Sofia, Bulgaria
³⁸ Faculty of Science, P.J. Šafárik University, Košice, Slovak Republic
³⁹ Frankfurt Institute for Advanced Studies, Johann Wolfgang Goethe-Universität Frankfurt, Frankfurt, Germany
⁴⁰ Fudan University, Shanghai, China
⁴¹ Gangneung-Wonju National University, Gangneung, Republic of Korea
⁴² Gauhati University, Department of Physics, Guwahati, India
⁴³ Helmholtz-Institut für Strahlen- und Kernphysik, Rheinische Friedrich-Wilhelms-Universität Bonn, Bonn, Germany
⁴⁴ Helsinki Institute of Physics (HIP), Helsinki, Finland
⁴⁵ High Energy Physics Group, Universidad Autónoma de Puebla, Puebla, Mexico
⁴⁶ Horia Hulubei National Institute of Physics and Nuclear Engineering, Bucharest, Romania
⁴⁷ HUN-REN Wigner Research Centre for Physics, Budapest, Hungary
⁴⁸ Indian Institute of Technology Bombay (IIT), Mumbai, India
⁴⁹ Indian Institute of Technology Indore, Indore, India
⁵⁰ INFN, Laboratori Nazionali di Frascati, Frascati, Italy
⁵¹ INFN, Sezione di Bari, Bari, Italy
⁵² INFN, Sezione di Bologna, Bologna, Italy
⁵³ INFN, Sezione di Cagliari, Cagliari, Italy
⁵⁴ INFN, Sezione di Catania, Catania, Italy
⁵⁵ INFN, Sezione di Padova, Padova, Italy
⁵⁶ INFN, Sezione di Pavia, Pavia, Italy
⁵⁷ INFN, Sezione di Torino, Turin, Italy
⁵⁸ INFN, Sezione di Trieste, Trieste, Italy
⁵⁹ Inha University, Incheon, Republic of Korea
⁶⁰ Institute for Gravitational and Subatomic Physics (GRASP), Utrecht University/Nikhef, Utrecht, Netherlands
⁶¹ Institute of Experimental Physics, Slovak Academy of Sciences, Košice, Slovak Republic
⁶² Institute of Physics, Homi Bhabha National Institute, Bhubaneswar, India
⁶³ Institute of Physics of the Czech Academy of Sciences, Prague, Czech Republic
⁶⁴ Institute of Space Science (ISS), Bucharest, Romania
⁶⁵ Institut für Kernphysik, Johann Wolfgang Goethe-Universität Frankfurt, Frankfurt, Germany
⁶⁶ Instituto de Ciencias Nucleares, Universidad Nacional Autónoma de México, Mexico City, Mexico
⁶⁷ Instituto de Física, Universidade Federal do Rio Grande do Sul (UFRGS), Porto Alegre, Brazil
⁶⁸ Instituto de Física, Universidad Nacional Autónoma de México, Mexico City, Mexico
⁶⁹ iThemba LABS, National Research Foundation, Somerset West, South Africa
⁷⁰ Jeonbuk National University, Jeonju, Republic of Korea
⁷¹ Johann-Wolfgang-Goethe Universität Frankfurt Institut für Informatik, Fachbereich Informatik und Mathematik, Frankfurt, Germany
⁷² Korea Institute of Science and Technology Information, Daejeon, Republic of Korea
⁷³ KTO Karatay University, Konya, Turkey
⁷⁴ Laboratoire de Physique Subatomique et de Cosmologie, Université Grenoble-Alpes, CNRS-IN2P3, Grenoble, France
⁷⁵ Lawrence Berkeley National Laboratory, Berkeley, California, United States
⁷⁶ Lund University Department of Physics, Division of Particle Physics, Lund, Sweden
⁷⁷ Nagasaki Institute of Applied Science, Nagasaki, Japan
⁷⁸ Nara Women's University (NWU), Nara, Japan
⁷⁹ National and Kapodistrian University of Athens, School of Science, Department of Physics , Athens, Greece
⁸⁰ National Centre for Nuclear Research, Warsaw, Poland
⁸¹ National Institute of Science Education and Research, Homi Bhabha National Institute, Jatni, India
⁸² National Nuclear Research Center, Baku, Azerbaijan
⁸³ National Research and Innovation Agency - BRIN, Jakarta, Indonesia
⁸⁴ Niels Bohr Institute, University of Copenhagen, Copenhagen, Denmark
⁸⁵ Nikhef, National institute for subatomic physics, Amsterdam, Netherlands
⁸⁶ Nuclear Physics Group, STFC Daresbury Laboratory, Daresbury, United Kingdom
⁸⁷ Nuclear Physics Institute of the Czech Academy of Sciences, Husinec-Řež, Czech Republic

- ⁸⁸ Oak Ridge National Laboratory, Oak Ridge, Tennessee, United States
⁸⁹ Ohio State University, Columbus, Ohio, United States
⁹⁰ Physics department, Faculty of science, University of Zagreb, Zagreb, Croatia
⁹¹ Physics Department, Panjab University, Chandigarh, India
⁹² Physics Department, University of Jammu, Jammu, India
⁹³ Physics Program and International Institute for Sustainability with Knotted Chiral Meta Matter (SKCM2), Hiroshima University, Hiroshima, Japan
⁹⁴ Physikalischs Institut, Eberhard-Karls-Universität Tübingen, Tübingen, Germany
⁹⁵ Physikalischs Institut, Ruprecht-Karls-Universität Heidelberg, Heidelberg, Germany
⁹⁶ Physik Department, Technische Universität München, Munich, Germany
⁹⁷ Politecnico di Bari and Sezione INFN, Bari, Italy
⁹⁸ Research Division and ExtreMe Matter Institute EMMI, GSI Helmholtzzentrum für Schwerionenforschung GmbH, Darmstadt, Germany
⁹⁹ Saga University, Saga, Japan
¹⁰⁰ Saha Institute of Nuclear Physics, Homi Bhabha National Institute, Kolkata, India
¹⁰¹ School of Physics and Astronomy, University of Birmingham, Birmingham, United Kingdom
¹⁰² Sección Física, Departamento de Ciencias, Pontificia Universidad Católica del Perú, Lima, Peru
¹⁰³ Stefan Meyer Institut für Subatomare Physik (SMI), Vienna, Austria
¹⁰⁴ SUBATECH, IMT Atlantique, Nantes Université, CNRS-IN2P3, Nantes, France
¹⁰⁵ Sungkyunkwan University, Suwon City, Republic of Korea
¹⁰⁶ Suranaree University of Technology, Nakhon Ratchasima, Thailand
¹⁰⁷ Technical University of Košice, Košice, Slovak Republic
¹⁰⁸ The Henryk Niewodniczanski Institute of Nuclear Physics, Polish Academy of Sciences, Cracow, Poland
¹⁰⁹ The University of Texas at Austin, Austin, Texas, United States
¹¹⁰ Universidad Autónoma de Sinaloa, Culiacán, Mexico
¹¹¹ Universidade de São Paulo (USP), São Paulo, Brazil
¹¹² Universidade Estadual de Campinas (UNICAMP), Campinas, Brazil
¹¹³ Universidade Federal do ABC, Santo Andre, Brazil
¹¹⁴ Universitatea Nationala de Stiinta si Tehnologie Politehnica Bucuresti, Bucharest, Romania
¹¹⁵ University of Cape Town, Cape Town, South Africa
¹¹⁶ University of Derby, Derby, United Kingdom
¹¹⁷ University of Houston, Houston, Texas, United States
¹¹⁸ University of Jyväskylä, Jyväskylä, Finland
¹¹⁹ University of Kansas, Lawrence, Kansas, United States
¹²⁰ University of Liverpool, Liverpool, United Kingdom
¹²¹ University of Science and Technology of China, Hefei, China
¹²² University of South-Eastern Norway, Kongsberg, Norway
¹²³ University of Tennessee, Knoxville, Tennessee, United States
¹²⁴ University of the Witwatersrand, Johannesburg, South Africa
¹²⁵ University of Tokyo, Tokyo, Japan
¹²⁶ University of Tsukuba, Tsukuba, Japan
¹²⁷ Universität Münster, Institut für Kernphysik, Münster, Germany
¹²⁸ Université Clermont Auvergne, CNRS/IN2P3, LPC, Clermont-Ferrand, France
¹²⁹ Université de Lyon, CNRS/IN2P3, Institut de Physique des 2 Infinis de Lyon, Lyon, France
¹³⁰ Université de Strasbourg, CNRS, IPHC UMR 7178, F-67000 Strasbourg, France, Strasbourg, France
¹³¹ Université Paris-Saclay, Centre d'Etudes de Saclay (CEA), IRFU, Département de Physique Nucléaire (DPhN), Saclay, France
¹³² Université Paris-Saclay, CNRS/IN2P3, IJCLab, Orsay, France
¹³³ Università degli Studi di Foggia, Foggia, Italy
¹³⁴ Università del Piemonte Orientale, Vercelli, Italy
¹³⁵ Università di Brescia, Brescia, Italy
¹³⁶ Variable Energy Cyclotron Centre, Homi Bhabha National Institute, Kolkata, India
¹³⁷ Warsaw University of Technology, Warsaw, Poland
¹³⁸ Wayne State University, Detroit, Michigan, United States
¹³⁹ Yale University, New Haven, Connecticut, United States
¹⁴⁰ Yonsei University, Seoul, Republic of Korea

¹⁴¹ Zentrum für Technologie und Transfer (ZTT), Worms, Germany¹⁴² Affiliated with an institute covered by a cooperation agreement with CERN¹⁴³ Affiliated with an international laboratory covered by a cooperation agreement with CERN.